Biogeosciences Discuss., https://doi.org/10.5194/bg-2018-441
Manuscript under review for journal Biogeosciences
Discussion started: 16 October 2018

Biogeosciences Discussions Open Access EGU

Multi-trace element sea surface temperature coral reconstruction for the southern Mozambique Channel reveals teleconnections with the tropical Atlantic

Jens Zinke[1,2,3,4], Juan-Pablo D'Olivo[5,6], Johannes C. Gey[2], Malcolm T. McCulloch[5,6], J. Henrich Bruggemann[7], Janice M. Lough[4,5], Mireille M. M. Guillaume[8]

[1]School of Geology, Geography and Environment, University of Leicester, LE17RH, United Kingdom
[2]Institute for Geosciences, Freie Universitaet Berlin, Berlin, 12249, Germany
[3]Molecular and Life Sciences, Curtin University, Perth, WA, Australia
[4]Australian Institute of Marine Science, Townsville, QLD 4810, Australia
[5]The ARC Centre of Excellence for Coral Reefs Studies, Australia
[6]Oceans Graduate School and UWA Oceans Institute, The University of Western Australia, Crawley, WA6009, Australia
[7]UMR ENTROPIE Université de La Réunion-CNRS-IRD, Saint-Denis, France & Laboratoire d'Excellence CORAIL
[8]UMR BOrEA Muséum National d'Histoire Naturelle-SU-UCN-UA-CNRS-IRD, Paris, France & Laboratoire d'Excellence CORAIL

Correspondence to: Jens Zinke (jz262@leicester.ac.uk)

Abstract

Here we report seasonally resolved sea surface temperatures for the southern Mozambique Channel in the SW Indian Ocean based on multi-trace element temperatures proxy records preserved in two *Porites* sp. coral cores. Particularly, we assess the suitability of both separate and combined Sr/Ca and Li/Mg proxies for improved multi-element SST reconstructions. Overall geochemical records from Europa Island *Porites* sp. highlight the potential of Sr/Ca and Li/Mg ratios as high-resolution climate archives but also show significant differences in their response at this Indian Ocean tropical reef site. Our reconstruction from 1970 to 2013 using the Sr/Ca-SST proxy reveals a warming trend of 0.58 ± 0.1 °C in close agreement with instrumental data (0.47 ± 0.07 °C) over the last 42 years (1970 to 2013). In contrast the Li/Mg showed unrealistically large warming trends, most probably caused by uncertainties around different uptake mechanisms of trace elements Li and Mg and uncertainties in their temperature calibration. However, spatial correlations between the combined detrended Sr/Ca, and Li/Mg proxies compared to instrumental SST at Europa revealed robust correlations with local climate variability in the Mozambique Channel and teleconnections to regions in the Indian Ocean and southeastern Pacific where

Biogeosciences Discuss., https://doi.org/10.5194/bg-2018-441
Manuscript under review for journal Biogeosciences
Discussion started: 16 October 2018

surface wind variability appeared to dominate the underlying pattern of SST variability. The strongest correlation was found between our Europa SST reconstruction and instrumental SST records from the northern tropical Atlantic SST. Only a weak correlation was found with ENSO, with recent warm anomalies in the geochemical proxies coinciding with strong El Niño or La Niña. We identified the Pacific/North American (PNA) atmospheric pattern, which develops in the Pacific in response to ENSO, and the tropical North Atlantic SST as the most likely causes of the observed teleconnections with the Mozambique Channel SST at Europa.

1 Introduction

Ocean-atmosphere dynamics in the tropics are key drivers of large-scale climate phenomena, such as the El Niño-Southern Oscillation (ENSO) (Angell, 1990; Trenberth et al., 1998; Xie et al., 2010; Timmermann et al., 2018). Tropical climate variability has therefore a strong impact on regional and global climate teleconnections. These ocean-atmosphere dynamics are temporally variable and sensitive to small perturbations in sea surface temperature (SST) associated with natural and anthropogenic climate change. The oceans response to the combined effects of natural variability and greenhouse driven anthropogenic warming act at seasonal, interannual and multi-decadal scales. The complexity of the climate system at temporal and spatial scales; therefore, call for a comprehensive assessment of SST pattern change in historical times (Xie et al., 2010). To investigate changing tropical climate and model potential future scenarios, the modern climatology faces the challenge of improving climate data coverage, especially extending the limited time length of instrumental measurements. The earliest records of SST, measured by commercial ship traffic, mainly along trading routes, started in the mid-19th century. Only with the arrival of satellite technology in the 1980's have the oceans been covered in more detail. The limited number of observations and drop in data quality prior to the 1980's cause considerable uncertainties in our understanding of important climate interactions (Thompson et al., 2008; Pfeiffer et al., 2017). These limitations make the use of paleoclimate reconstructions, particularly from remote locations, a vital tool to learn about past climate conditions.

Coral reconstructions extending back decades to several centuries provide invaluable data to assess past tropical climate variability (Hennekam et al., 2018; Pfeiffer et al., 2017). One of the most robust and widely used geochemical proxies to reconstruct SST in tropical areas is

68 the Sr/Ca ratio from massive corals like *Porites* (Corrège, 2006; Pfeiffer et al., 2009; DeLong
69 et al., 2012). The Sr/Ca ratios in $CaCO_3$ precipitated during skeletal formation are negatively
70 correlated with temperatures, i.e. as temperatures increase, less Sr is incorporated into the
71 aragonite lattice relative to Ca (Alibert and McCulloch, 1997; Corrège, 2006; DeLong et al.,
72 2007). While the Sr/Ca proxy is a remarkably useful tool for paleoclimate reconstructions,
73 there are a number of limitations that need to be considered in the application of this proxy
74 for quantitative reconstructions. Among these, there is a significant difference in the Sr/Ca
75 temperature dependency of biogenic and experimentally precipitated inorganic aragonite
76 (Smith et al., 1979). Abiogenic aragonite has a significantly stronger Sr/Ca dependence to
77 temperature with a slope of -0.039 to -0.044 mmol/mol per °C than the coral skeletal Sr/Ca
78 with slopes ranging between -0.040 to -0.084 mmol/mol per °C (Smith et al., 1979; Cohen et
79 al., 2002; Gaetani & Cohen, 2006; Gaetani et al., 2011; De Carlo et al., 2015). This disparity
80 has been considered as the influence of strong "vital effects" during the coral
81 biomineralization process or bio-smoothing effects (de Villiers et al., 1995; Gagan et al.,
82 2012). Nevertheless, several recent studies have confirmed the suitability of the Sr/Ca
83 paleorecorder when carefully sampled along the optimal growth axis and ideally replicated
84 (Pfeiffer et al., 2009, 2017; De Long et al., 2012; Zinke et al., 2016). Recently, the use of
85 additional SST sensitive proxies (multi-element paleothermometry) has been tested and the
86 Li/Mg ratios emerged as a promising tool to reconstruct SST (Hathorne et al., 2013;
87 Montagna et al., 2014; D'Olivo et al., 2018). The innovation of the Li/Mg temperature proxy
88 lies in the normalization of Li to Mg which is thought to eliminate the influence of Raleigh
89 fractionation processes influencing most trace element incorporations into the coral skeleton
90 (Cohen et al., 2002; Gaetani & Cohen, 2006; Gaetani et al., 2011). Li/Mg was shown (e.g.
91 Montagna et al., 2014) to be applicable to a large range of coral species inhabiting a large
92 temperature range. However, to date no long-term (e.g multi-decadal) SST reconstruction has
93 been developed based on Li/Mg ratios to test its suitability, particularly in tropical corals, in
94 comparison to the established Sr/Ca time series.

95 The aim of this study was to reconstruct sea surface temperatures based on coral Sr/Ca,
96 Li/Mg and their combination to validate and extend the SST information for the southern
97 Mozambique Channel in the southwestern Indian Ocean. We examined instrumental climate
98 and coral proxy data from Europa Island. The high latitude of this atoll and the lack of human
99 impact make this location ideal to investigate past climate variability based on cores from
100 massive *Porites* corals (Fig. 1). The Mozambique Channel in the southwestern Indian Ocean

is a particular sparsely sampled region, despite its importance as a major pathway of warm surface flow of the global ocean conveyer (De Ruijter et al., 2002; Schouten et al., 2002; Woodruff et al., 2011; Beal et al., 2011). Furthermore, Europa Is. is located just upstream of the region that feeds the Agulhas Current, one of the most powerful western boundary currents on the planet. As such, this region is a possible source of both local and global climate interactions and drivers of especially longer-term changes in patterns of SST variability, which are investigated here.

2 Materials and Methods

2.1 Study area

Europa Is. (hereafter Europa), a 28 km^2 atoll that is part of the five *Eparses* Islands, of the French *Terres Australes et Antarctiques Françaises,* and lies in the central Mozambique Channel between southern Mozambique and southern Madagascar (22° 21' S, 40° 21' E; Fig. 1). Europa, with Hall Tablemount and Bassas da India Atoll, is part of an archipelago that was hypothesized to have been formed by the Quathlamba hotspot, which presently lies beneath Lesotho (Hartnady, 1985). Europa is a carbonate platform attaining a maximum elevation of 6 m with a fossil coral terrace that was dated to the last interglacial period with an age of approximately 94 kyr (Battistini et al., 1976), therefore formed concomitantly to other carbonate platforms in the Mozambique Channel (Battistini et al., 1976; Guillaume et al., 2013). The 22 km coastline is surrounded by a fringing coral reef with a fore reef slope that dips steeply into deeper water. A geomorphological relict of the former atoll drained by the following marine regression forms a narrow shallow lagoon that occupies more than the half of the island and opens to the sea through the northern reef flat. A mangrove formation ranging from shrub to forest stands grows in the salt waters of the back and windward edge of the lagoon (Lambs et al., 2016). Europa is characterized by a high-energy environment under the influence of south to southeasterly trade winds (strongest in austral winter) and occasionally impacted by tropical cyclones in austral summer (Barruol et al., 2016). A train of anticyclonic ocean eddies traveling through the Mozambique Channel transports tropical water southward eventually feeding the Agulhas Current (Beal et al., 2011).

Europa is a no-take area; the pristine state of its fringing coral reefs was attested by scarce macroalgae, high fish biomass and high coral coverage that locally exceeded 100% in 2013 due to superimposed platy *Acropora* stands (Guillaume & Bruggemann 2011). While almost undisturbed from local anthropogenic disturbance, remote islands are impacted by global

change. For instance in 1998 (El Niño) a severe coral bleaching event was inferred at Europa from a high coral mortality accompanied by a recruit cohort of small-sized *Acropora* colonies observed 4 years later (Quod & Garnier 2004). In 2011 (La Niña), a moderate bleaching event affecting mostly *Pocillopora* corals, massive and branching *Porites* was witnessed (Guillaume & Bruggemann 2011).

2.2 Instrumental temperature data

To review and evaluate the coral geochemical proxies, various types instrumental data were assessed. High-resolution SST data (0.25° × 0.25°) covering 1981 to 2013 was obtained from the Advanced Very High Resolution Reconstructed Optimum Interpolation Sea Surface Temperature version 2 (AVHRR-OISSTv2; Banzon et al., 2014, 2016; Reynolds et al., 2007). The AVHRR-OISSTv2 dataset is composed of daily satellite data and in *situ* data, adjusted for biases (Banzon et al., 2014). The SST data was extended back to 1970 using the Extended Reconstructed Sea Surface Temperature (ERSSTv4; Liu et al., 2015) dataset, which is based on the "International Comprehensive Ocean-Atmosphere Data Set" (ICOADS; Woodruff et al., 2011). The ESRSSTv4 record is composed of satellite data from the AVHRR data extended with temperature records from ships and buoys processed at monthly resolution and interpolated to a spatial resolution of 2.0 degrees. In addition, *in situ* SST data was available from April 2009 to October 2010 measured by a tide-temperature-conductivity XR-420 6.30 RBR Ltd gauge deployed by the CNRS-INSU close to the *Porites* coral coring site studied here (Testut et al., 2016). Finally, *in situ* air temperature records were provided by the Meteo-France station at Europa (n° 98403003, 22.32 °S, 40.33 °E, elevation 6 m).

2.3 Coral core sampling, analysis and age model

Coral cores were extracted with a pneumatic drill from two living massive *Porites* colonies on the northeastern reef slope of Europa in early May 2013 during the *ORCIE* scientific expedition. The cores were obtained at a depth of 12 m to 13 m in sections of ~30 cm. Morphological identification based on skeletal features observed under an optical microscope assigned core EU3 to *P. solida* and core EU2 to *P. mayeri*. The longest core EU3 measured 136 cm (Table 1) and was sampled from 2013 back to 1970. The shorter core EU2 was sampled from 2013 back to 2003. Cores were sliced to 7 mm thick slabs and cleaned following established protocols (Nagtegaal et al., 2012). The slabs were then X-rayed to

reveal the annual density banding and analysed by densitometry at the Australian Institute of Marine Science (Figs. S1 & S2). Annual rates of linear extension were calculated from 1) X-ray based density measurements with coral XDS software and 2) the bimonthly Sr/Ca records by measuring the distance between Sr/Ca maxima in both records.

The basis for the optimal extraction of geochemical signals from massive *Porites* is the precise selection of the sampling path, according to the architecture of the coral skeleton. The X-rays show the corallite fan structures with the chosen sampling path along the central growth axis of the corallum highlighted (Figs. S1 & S2). Carbonate powder samples of approximately 50 mg at 2 mm continuous intervals were obtained along this sampling path with a 0.9 mm diameter dental drill. Processing of the samples for geochemical analysis is based on methods described by Zinke et al. (2015) and D'Olivo et al. (2018). First the powder samples were homogenized in a small agate mortar and ~10 mg were weighed into thoroughly cleaned 5-ml tubes. Subsequently the samples were dissolved in 0.5 ml of 0.5 N HNO3 and diluted to a calcium concentration of 100 ppm by taking an aliquot of 38 ml from the primary dissolution and adding 3 ml of 2 % HNO_3 and used for the analysis of Li and Mg. A second aliquot for the analysis of Sr, Ca, and Mg was prepared at 10 ppm by using a 300 ml aliquot of the first dilution and adding 2.7 ml of 2 % HNO_3 spiked with trace concentrations of scandium, praseodymium and yttrium used as internal standards. The analyses for trace element concentrations (TE) were made on a Thermo Scientific XSERIES 2 quadrupole ICP-MS (inductively coupled plasma mass spectrometer) at the University of Western Australia (UWA). The Sr/Ca data reported here are normalized to the JCp-1 *Porites* sp. standard prepared by the Geological Survey of Japan (Okai et al., 2002) with Sr/Ca = 8.838 mmol/mol. Long-term reproducibility was determined using the UWA *in-house* Davies Reef coral standard solution with Mg/Ca = ±6.2%, Sr/Ca = ±0.4%, and U/Ca = ±1.1% (2σ RSD; n=167) (D'Olivo et al., 2018).

The first step after generating the trace element records was to assign an age model. The 2 mm sampling resolution provided 6 to 9 samples per year for any given year and provided robust bimonthly resolved geochemical records. Based on the instrumental SST data from AVHRR-OI SST and the *in situ* measurements August was established the coldest month for our location. The highest Sr/Ca annual values in the raw data were tied with the annual minimum in the SST records using the open source time series analysis toolkit "Analyseries".

199 Bimonthly (6 samples per year) records were generated by linear interpolation in Analyseries
200 to facilitate comparisons between the different datasets.

201 Ordinary linear least squares regression (OLS) was used to calibrate the geochemical ratios
202 with the SST products. In addition to absolute SST values, SST anomalies (deviations from
203 bimonthly SST seasonality in any given year) were calculated relative to the reference period
204 of 2003 to 2013, which includes the overlap between both cores. Longer time series
205 anomalies were calculated relative to the 1981 to 2010 period. Bimonthly temperature
206 residuals were calculated for absolute SST and SST anomaly reconstructions to highlight
207 periods where Sr/Ca-SST and Li/Mg-SST differ from instrumental SST. To evaluate how
208 different trace element ratios track instrumental temperatures, uncertainties in bimonthly
209 absolute SST and SST anomalies for individual and composite cores were calculated based
210 on the root mean square error (RMSE) defined as:

211 $$RSME = \sqrt{\frac{1}{N}\Sigma\left(T_{calc,n} - T_{meas,n}\right)^2},$$

212

213 where $T_{calc,n}$ is the n'th term from the coral derived temperature and $T_{meas,n}$ is the n'th
214 measurement in the instrumental record and N is the total number of observations.

215

216 **3 Results**

217 **3.1 Bimonthly Sr/Ca, Li/Mg, Mg/Ca and Li/Ca ratios**

218 The bimonthly time series of all trace element ratios measured in cores EU2 and EU3 are
219 illustrated in Figure 2. Comparisons between the different trace element ratios for the period
220 of overlap between 2003 and 2012 are shown in Figure 3 and Table S1.

221 For the period of overlap the bimonthly time series of the Sr/Ca ratios of core EU3 ranged
222 between 8.78 and 9.03 mmol/mol (8.77 and 9.09 mmol/mol between 1970 and 2012) and in
223 EU2 between 8.90 and 9.18 mmol/mol (Fig. 2a; Fig. 3a). The mean Sr/Ca ratios of the EU2
224 core were ~0.1 mmol/mol higher compared to EU3, while seasonal amplitudes and trend
225 since 2003 were similar between cores (Fig. 2a). Sr/Ca ratios for EU2 and EU3 were highly
226 correlated ($r^2 = 0.85$, $p < 0.001$, $N = 54$). Both cores showed a long-term decrease (warming
227 trend) in Sr/Ca between 2003 and 2012. The time series of EU3 Sr/Ca between 1970 and
228 2012 showed a non-linear decrease starting in the mid to late-1990s with the records lowest
229 ratios between 1998 and 2000 and 2009 to 2011.

230 The seasonal range in Li/Mg ratios in core EU3 varied between 1.18 and 1.52 mmol/mol
231 (1.18 and 1.65 mmol/mol between 1970 and 2012) while in core EU2 it ranges between 1.35
232 and 1.6 mmol/mol and showed an offset to higher absolute Li/Mg ratios between 2003 and
233 2012 (Fig. 2b, Fig. 3a). Li/Mg between EU2 and EU3 were highly correlated ($r^2 = 0.69$, $p <$
234 0.001, N = 54), although lower than Sr/Ca ratios. The time series of EU3 Li/Mg between
235 1970 and 2012 showed a non-linear decrease starting in the mid to late-1990s. For the period
236 of overlap between 2003 and 2012, both core Li/Mg ratios showed no trend.

237 Mg/Ca ratios in core EU3 showed larger amplitude seasonal variations than core EU2 (Fig.
238 2c). EU2 Mg/Ca ratios ranged between 4.24 and 4.61 mmol/mol between 2003 and 2012
239 while EU3 ranged between 4.40 and 5.36 mmol/mol (4.03 and 5.36 mmol/mol between 1970
240 and 2012; Fig. 2c, Fig. 3b). EU2 showed lower mean Mg/Ca ratios (~0.4 mmol/mol) than
241 EU3 between 2003 and 2012 (Fig. 3b). Mg/Ca ratios in EU2 and EU3 were well correlated,
242 yet significantgly lower than Sr/Ca and Li/Mg ($r^2 = 0.34$, $p < 0.001$, N = 54). Overall, EU3
243 Mg/Ca showed an increase since 1970 with a marked switch post-2005. EU2 Mg/Ca had no
244 trend.

245 Li/Ca ratios in core EU2 ranged between 6.03 and 7.20 μmol/mol while in EU3 it ranged
246 between 6.04 and 6.87 μmol/mol (5.97 to 6.87 μmol/mol between 1970 and 2012; Fig. 2d,
247 Fig. 3c). Li/Ca ratios in EU2 and EU3 were well correlated ($r^2 = 0.33$, $p < 0.001$, N = 54), yet
248 significantly lower than Sr/Ca and Li/Mg. Li/Ca was positively correlated with Sr/Ca and
249 Li/Mg and negatively with Mg/Ca in both cores for most of the record (Figs. 3c, e, f; Table
250 S1). EU2 Li/Ca largely mirrored variations in Sr/Ca and Li/Mg, while in EU3 Li/Ca showed
251 lower correlations (Table S1). EU3 interannual variability in Li/Ca deviated from the patterns
252 observed in the Sr/Ca, Li/Mg and Mg/Ca data in 1970/71, 1976-78, 1989/90 and between
253 2001 and 2004 (Fig. 2d). In those years lower EU3 Li/Ca ratios were associated with lower
254 Mg/Ca and higher Sr/Ca and Li/Mg ratios, opposite to the expected relationships (Fig. 2d).

255

256 **3.2 Calibration of TE/Ca and SST reconstruction**

257 Absolute temperature reconstructions were obtained from the regression of the bimonthly
258 Sr/Ca and Li/Mg ratios with the AVHRR-OISSTv2 and ERSSTv4 data (Fig. 4; Table 2; for
259 ERSSTv4 see Fig. S3 and for Mg/Ca and Li/Ca vs. SST see Fig. S4). Both of the coral
260 datasets showed highly significant ($p<0.001$) correlation coefficients with the temperature

261 products over the period of overlap (2003 to 2012) with $r^2_{EU3\ Sr/Ca} = 0.92$, $r^2_{EU2\ Sr/Ca} = 0.93$,
262 $r^2_{EU3\ Li/Mg} = 0.78$ and $r^2_{EU2\ Li/Mg} = 0.93$ (Table 2). The Sr/Ca and Li/Mg time series of cores
263 EU3 and EU2 were highly consistent in the period of overlap (2003 to 2012). EU2 Sr/Ca and
264 Li/Mg performed equally well in the regressions, while EU3 Li/Mg slightly underperformed
265 Sr/Ca (Fig. 4; Table 2). Correlation coefficients of EU3 Sr/Ca and Li/Mg for the longer
266 periods 1981 to 2012 and 1970 to 2012 with AVHRR-OISSTv2 and ERSSTv4, respectively,
267 were also high (Table 2; Fig. S5). The regression slope of TE ratios with the two SST
268 products varied between -0.040 and -0.051 mmol/mol per °C for Sr/Ca and between -0.045
269 and -0.064 mmol/mol per °C for Li/Mg (Table 2). Overall, the regression slopes were
270 marginally lower for regressions with AVHRR-OISSTv2 compared to ERSSTv4. Linear
271 OLS regressions with 1.5 years *in situ* SST data between 2009 and 2010 revealed similar
272 regression slopes for Sr/Ca and Li/Mg but with narrower range (-0.042 to -0.047 mmol/mol
273 per °C for Sr/Ca and –0.045 to -0.052 mmol/mol per °C for Li/Mg) and lower correlation
274 coefficients ($r^2_{EU3\ Sr/Ca} = 0.70$, $r^2_{EU2\ Sr/Ca} = 0.76$, $r^2_{EU3\ Li/Mg} = 0.73$ and $r^2_{EU2\ Li/Mg} = 0.81$). All
275 correlations were statistically significant with $p < 0.05$.

276 The maximal seasonal range over the period 1970 to 2012 of the reconstructed bimonthly
277 Sr/Ca-SST and Li/Mg-SST varied between 22 °C and 30 °C in both cores with a mean
278 seasonal amplitude of 4.33±0.67 °C (Fig. 5; for ERSST4 see Fig. S5) in close agreement with
279 *in-situ* SST (4.82±0.05 °C for 2009 to 2010) and regional AVHRR-OISSTv2 (4.67±0.7 °C
280 for 1981 to 2013) and ERSSTv4 (4.52±0.44 °C for 1970 to 2012).

281 Residuals (calculated as the difference between coral-derived SST and AVHRR-OISSTv2 for
282 individual record length) are presented in Fig. 5 and RMSE's in Table 3 (for ERSSTv4 see
283 Fig. S5). The coral Sr/Ca and Li/Mg-SST reconstructions had the lowest residuals between
284 1993 and 2012 with AVHRR-OISSTv2, with slightly larger residuals prior to 1993 (core
285 EU3). AVHRR-OISSSTv2 displayed a more limited seasonality between 1989 and 1995
286 (warmer winters) with on average higher mean SST than coral-derived SST (Fig. 5; Sr/Ca,
287 Li/Mg and their combination). Summer SST (Sr/Ca, Li/Mg and their combination) was in
288 general in better agreement throughout the individual records. Sr/Ca performed best as SST
289 proxy followed by the combined Sr/Ca and Li/Mg-SST (Fig. 5; Table 3).

290 Sr/Ca, Li/Mg and SST bimonthly anomalies were calculated relative to the 2003 to 2012
291 (core overlap) and 1981 to 2010 (coral composite) reference period. Coral-derived SST
292 anomalies were calculated using the literature average proxy-SST relationships of -0.0607

mmol/mol per °C for Sr/Ca (Corrège, 2006) and -0.060 mmol/mol per °C for Li/Mg (for *Porites* growing within 25 and 30 °C; Hathorne et al., 2013; D'Olivo et al., 2018), both within the range of regression slopes obtained for our Europa cores. Composite coral-derived SST anomalies were then calculated as the arithmetic mean obtained from the two cores. Residuals were calculated as the difference between coral-derived SST anomalies and AVHRR-OISSTv2 anomalies (for ERSSTv4 see Fig. S6).

Figure 6 illustrates the anomalies (1981 to 2010) for the composite proxy SST from the two cores (individual cores shown in Fig. S6) compared to the SST anomalies from AVHRR-OISSTv2 (for ERSSTv4 see Fig. S7). EU2 and EU3 Sr/Ca and Li/Mg anomalies agreed well between records ($r_{Sr/Ca}$ = 0.46, p <0 .001, N = 57; $r_{Li/Mg}$ = 0.56, p < 0.001, N = 57; Fig. S7). The amplitudes of the EU Sr/Ca-SST composite anomalies closely tracked AVHRR-OISSTv2 anomalies with slightly higher residuals prior to 1993 (Fig. 6a). EU Li/Mg-SST composite anomalies displayed similar variability as AVHRR-OISSTv2, yet the agreement was slightly lower than for Sr/Ca-SST anomalies with a shift to lower mean Li/Mg-SST ($r_{Sr/Ca}$ = 0.37, p < 0.001, N = 189; $r_{Li/Mg}$ = 0.33, p<0.001, N = 189; Fig. 6b). The detrended bimonthly records agreed well between composite Sr/Ca-SST and Li/Mg-SST anomalies (r = 0.73, p < 0.001, N = 252) and with AVHRR-OISSTv2 anomalies ($r_{Sr/Ca}$ = 0.41, p < 0.001, N = 189; $r_{Li/Mg}$ = 0.31, p < 0.001, N=189). As with absolute SST, Sr/Ca-SST and Li/Mg-SST composite anomalies showed larger residuals pre-1993 and in general cooler anomalies than in AVHRR-OISSTv2 (Fig. 6c; for ERSSTv4 see Fig. S7). The lowest residuals were found for Sr/Ca-SST and Sr/Ca-Li/Mg combined SST anomalies (Fig. 6c, d). RMSE's between 2003 and 2012 are lowest for Sr/Ca-SST (0.49±0.35 °C) followed by Sr/Ca-Li/Mg (0.76 ± 0.39 °C) and Li/Mg-SST (1.03±0.50 °C) while RMSE's between 1970 and 2012 are slightly higher (Table 3).

The anomalies for the EU Sr/Ca-SST, Li/Mg-SST and Sr/Ca-Li/Mg-SST composite time series closely tracked the anomalies in the *in situ* air temperature data (Figs. 7a-c). Sr/Ca-SST and Sr/Ca-Li/Mg-SST performed slightly better than Li/Mg-SST ($r_{Sr/Ca}$ = 0.46, p < 0.001, N = 189; $r_{Sr/Ca\text{-}Li/Mg}$ = 0.43, p < 0.001, N = 189; $r_{Li/Mg}$ = 0.37, p < 0.001, N = 189). Air temperatures showed marginally cooler temperature anomalies between 1970 and 1978 compared to the Sr/Ca, Li/Mg or Sr/Ca-Li/Mg composite SST anomalies. AVHRR-OISSTv2 was also in close agreement with air temperature anomalies (Fig. 7d). ERSSTv4 anomalies mirrored air temperatures with overall slightly cooler mean SST anomalies than in air temperatures, especially between 1970 and 1990 (Fig. 7e).

326

327 **3.3. Coral growth parameters and SST**

328 Linear extension rates based on the distance between annual density bands and the distance
329 between Sr/Ca maxima in both cores displayed interannual and multi-decadal variability (Fig.
330 8b; for anomalies see Fig. S8). Linear extension for EU3 was within 0.2 cm between the two
331 methods except during 1972 to 1973 and 1983 to 1985. The exceptionally low extension rates
332 during these intervals obtained in core EU3 by the density method were most probably
333 related to uncertainties in defining the chronology due to poorly defined density contrasts.
334 Therefore, for those years, the clear seasonal pattern in Sr/Ca provided a better chronology
335 control than X-ray densitometry. Extension rates measured with the density method in EU2
336 and EU3 between 1968 and 2012 showed similar values, with a mean of 1.16±0.33 cm/yr for
337 EU2 and 1.2±0.27 cm/yr for EU3, However, the sclerochronology based on the density
338 measured with X-rays had large uncertainties due to poorly defined annual density cycles in
339 EU2 in the older part of the record. EU2 and EU3 mean extension rates measured between
340 Sr/Ca maxima between 2003 and 2012 were also similar with 1.23±0.14 cm/yr for EU2 and
341 1.28±0.13 cm/yr for EU3 (Fig. 8). Interannual extension rates in EU2 and EU3 showed no
342 significant correlation.

343 Skeletal density in core EU3 displayed lower variability (±0.1 g/cm^3) than core EU2 (±0.2
344 g/cm^3) with no correlation between cores and no significant trend (Fig. 8c). Interestingly,
345 core EU2 displayed higher density than EU3 in El Niño years 1977/78, 1982/83, 2002/03 and
346 2010. EU3 and EU2 density variations were in anti-phase with extension rates for most of the
347 record. Variability and trends in calcification in both cores were mainly explained by changes
348 in extension rates.

349 We find no correlation between SST reconstructions or instrumental SST with either
350 extension or calcification rates nor skeletal density in both cores (Fig. 8a). The period of
351 fastest extension and highest calcification in EU3 corresponded to 1947 to 1961. No
352 significant changes in extension or calcification rates were associated with known El Niño
353 events (e.g. 1941/42 and 1998) or local cold/warm events recorded by instrumental and proxy
354 records (e.g. 1994, 2002).

355 **3.4 Regional and large-scale climate relationships**

356 To assess regional correlations, we compared the EU Sr/Ca-SST composite with published
357 coral proxy records from the Mozambique Channel and their corresponding instrumental data
358 based on ERSSTv4 (Fig. 9; Fig. S9). The proxy records included *Porites* coral oxygen
359 isotope and Sr/Ca from Mayotte (Comoros Archipelago; 13° S, 45° E; Zinke et al., 2008) in a
360 lagoonal setting and from Ifaty Reef in a lagoon passage (Southwest Madagascar, 23° S, 43°
361 E; Zinke et al., 2004). Bimonthly anomalies for ERSSTv4, Sr/Ca-SST and δ^{18}O-SST were
362 calculated relative to the reference period 1973 to 1993. The ERSSTv4 records from the three
363 sites, spanning 10° of latitude in the Mozambique Channel between 13° and 23° S,
364 documented a statistically significant (>95%) warming trend since 1970 (Fig. 9). ERSSTv4
365 for 2° × 2° spatial grids near Europa and Ifaty Reef shared 98% of variability, while Mayotte
366 shared 38% of variability with the former two sites. The coral proxy-based SST anomalies
367 also showed statistically significant (>95%) warming trends, although generally higher than
368 in ERSSTv4, with the exception of Ifaty that showed no trend in Sr/Ca-SST anomalies (Fig.
369 9).

370 The interannual variability in the EU Sr/Ca-SST composite anomalies and in the Mayotte and
371 Ifaty proxy-SST anomalies fluctuated by ~±1 °C with the exception of a few warm and cold
372 spikes in Mayotte and Ifaty time series which were not recorded at Europa (Fig. 9b-e; Fig.
373 S9). The EU Sr/Ca-SST composite anomalies agreed best with interannual variability in Ifaty
374 Sr/Ca-SST ($r = 0.42$, $p < 0.001$, $N = 21$) and δ^{18}O-SST ($r = 0.19$, $p < 0.05$, $N = 21$), although
375 with a cold bias in Ifaty Sr/Ca between 1985 and 1995 (Fig. 9d,e; Fig. S9). The EU Sr/Ca-
376 SST composite anomalies and Mayotte proxy-SST anomalies showed no significant
377 correlations, although the trend estimates were within uncertainty bounds for Mayotte δ^{18}O-
378 SST (Fig. 9b,c; Fig. S9). Mayotte Sr/Ca time series showed anomalous cold spikes between
379 1970 and 1978, which were not recorded in regional ERSSTv4 (Fig. S9b,c).

380 Spatial correlations between the EU composite SST anomalies and the AVHRR-OISSTv2
381 mean annual averages (July to June) between 1981 and 2012 (Fig. 10) for each grid point
382 were calculated to investigate large-scale teleconnections. Similar spatial correlations were
383 calculated with the AVHRR-OISSTv2 data near Europa at 22° S, 40° E (1° × 1° resolution)
384 with the rest of the grid points (Fig. 10). The correlations of the detrended data were
385 computed using the KNMI climate explorer (https://climexp.knmi.nl/; Trouet & Oldenborgh,
386 2005) with a cutoff p-value < 0.05. Similar correlation patterns were observed for the
387 EU2/EU3 Sr/Ca-Li/Mg SST composite and the local AVHRR-OISSTv2 with global grids in

AVHRR-OISSTv2 (Figs. 10a-b). Coherent positive correlation patterns emerge in the Mozambique Channel, the northern and southeastern Indian Ocean, the southeastern tropical Pacific and northern tropical Atlantic. The Sr/Ca and Li/Mg ratios showed the expected negative relationship of both proxies with regional AVHRR-OISSTv2 mirroring the SST patterns (Figs. 10c-d). Of particular interest was the strong relationship with the northern tropical Atlantic (0° N to 20° N, 80° W to 30° W).

The regressions of detrended coral composite Sr/Ca and Sr/Ca-Li/Mg combined SST reconstructions with northern tropical Atlantic AVHRR-OISSTv2 revealed the strongest positive relationships for annual means between July and June (Table 4). Correlations between detrended coral composite Li/Mg-SST reconstructions with northern tropical Atlantic AVHRR-OISSTv2 were slightly lower. Northern tropical Atlantic AVHRR-OISSTv2 (1981 to 1970) and ERSSTv4 (1970 to 2017) showed positive correlations with the Atlantic Multi-decadal Oscillation (AMO) index ($r = 0.7$ to 0.72, $p < 0.001$; Table 4). Our detrended coral composite Sr/Ca and Sr/Ca-Li/Mg combined SST reconstructions also showed statistically significant positive correlations with the AMO index based on ERSSTv4 (Table 4). However, AVHRR-OISSTv2 and ERSSTv4 for Europa indicated low or non-significant correlations with the AMO, respectively, despite the strong correlations with the northern tropical Atlantic (Table 3). Furthermore, the Tropical North Atlantic (TNA; Enfield et al., 1999) and North Tropical Atlantic indices (NTA; Penland & Matrosova, 1998) indicated statistically significant positive correlations with the coral-based SST and instrumental SST data at Europa (Fig. 10e; Table 4).

The regressions of detrended seasonal averages in AVHRR-OISSTv2 for Europa with the Niño3.4 index of ENSO variability showed weak, yet statistically significant correlations in the season from February to April ($r = 0.47$; $p < 0.01$; Table 4). The correlations between ERSSTv4 and Niño 3.4 were weaker ($r = 0.34$, $p < 0.05$; Table 4). The detrended coral composite Sr/Ca, Li/Mg and their combined SST reconstructions showed no significant correlations with the Niño3.4 index. However, the Pacific/North American (PNA) pattern (Wallace & Gutzler, 1981), which is an atmospheric response to ENSO, showed statistically significant correlations with AVHRR-OISSTv2 ($r =0.67$, $p < 0.001$) for Europa and the coral-derived SST anomalies between 1981 and 2012 ($r = 0.42$, $p = 0.014$; Table 4). The spatial correlation pattern of the PNA index with global AVHRR-OISSTv2 revealed a similar pattern as observed for the coral-based SST (Fig. 10).

Biogeosciences Discuss., https://doi.org/10.5194/bg-2018-441
Manuscript under review for journal Biogeosciences
Discussion started: 16 October 2018

420

421 **4 Discussion**

422 **4.1 Reliability of Sr/Ca and Li/Mg as SST proxies**

423 Both of the Europa coral core Sr/Ca and Li/Mg bimonthly time series (EU3 and EU2)
424 showed highly significant correlations with the local and regional instrumental SST products
425 (AVHRR-OISSTv2 and ERSSTv4). For the period of overlap between 2003 and 2012 both
426 proxies performed equally well in core EU2 while core EU3 Li/Mg slightly underperformed
427 Sr/Ca. The regression slopes with SST were within the range of published calibrations for
428 *Porites* corals (e.g. Hathorne et al., 2013; Montagna et al., 2014; D'Olivo et al., 2018). The
429 bimonthly Sr/Ca, Li/Mg and combined Sr/Ca-Li/Mg absolute SST reconstructions showed
430 small deviations (mean RMSE's between 0.45 and 0.67°C; Table 3) from the instrumental
431 temperatures with lower winter and slightly higher summer SST. For all proxies the
432 agreement with instrumental data was highest for the period of overlap between cores (2003
433 and 2012). In general, AVHRR-OISSTv2 seasonal SST amplitudes and SST anomalies
434 showed higher correlations with the coral-based SST reconstructions than with ERSSTv4.
435 The lower temperatures in the proxy-SST compared with the satellite data of AVHRR-
436 OISSTv2, which measures SST at the skin of the sea surface (top few millimeters), could be
437 related to the living depth of the corals (12 to 13 m). This was particularly apparent in several
438 cold spikes with 2S.D. (-0.72 °C) below the 1981 to 2012 mean SST in our coral-based SST
439 anomaly reconstructions, which were also observed in the instrumental data (1971, 1972,
440 1976, 1978, 1980, 1984, 1986, 1994, 2001, 2008). The most extreme cold excursions during
441 austral summer occurred in 1986, 1994, 2001 and 2008, which were also prominent in the
442 AVHRR-OISSTv2. 1994 stands out as the coldest anomaly between 1970 and 2012 in coral-
443 based SST (-1.34 °C), AVHRR-OISSTv2 (-1.37 °C) and ERSSTv4 (-1.16 °C). However,
444 January/February 1989 and March-June 1997 cold spikes exceeding 1 °C observed in
445 AVHRR-OISSTv2 were not as extreme in our coral-based SST anomalies (-0.58 °C in 1989;
446 -0.1 °C in 1997). A possible explanation for these cold spikes is the upwelling of colder
447 deeper water onto the north-east coast reef promoted by the steep slopes and topography of
448 the fore-reef (gentle sloping plain to a depth of 25m). Upwelling-related cold spikes have
449 been recorded in temperature loggers across the Mozambique Channel at 18 m depth,
450 potentially related to periods of active Mozambique Channel eddies interacting with the steep
451 topography (Schouten et al., 2002; Swart et al., 2010; Van den Berg et al., 2007). Differences

between the proxy records and the instrumental records at interannual scales could also reflect limitation in the instrumental records. The ERSSTv4 data used extending back to 1970 is based on very sparse observations in the ICOADS database for the southern Mozambique Channel. The resolution of the satellite data starting in 1981 should provide the best estimates for SST near Europa; however, observations near the coast can be susceptible to biases (e.g. mixing of land temperature with SST; Brevin et al. 2017; Smit et al., 2013). The comparison between AVHRR-OISSTv2 and local air temperature anomalies revealed an excellent agreement for the years covered by the weather station and serves as a quality check for the AVHRR-OISSTv2 data for our site. Nevertheless, the absolute temperature reconstruction from the coral Sr/Ca and Li/Mg ratios showed a good agreement with the different instrumental temperature datasets. Thus, both Sr/Ca and Li/Mg provide highly reliable SST proxies and in combination have the potential to improve SST reconstructions.

The statistically significant warming-trend of 0.58 ± 0.1 °C ($p < 0.001$) between 1970 and 2012 in the coral Sr/Ca-SST composite was in close agreement with instrumental SST data (0.47 ± 0.07 °C in ERSSTv4; 0.40 ± 0.18 °C in AVHRR-OISSTv2 since 1981). The Li/Mg-SST composite trend of 1.06 ± 0.15 °C ($p < 0.001$) is however too large, and inconsistent with both the Sr/Ca and instrumental records. The differences in warming trends in Li/Mg-SST and Sr/Ca-SST probably highlight the differences in incorporation between these elements (Montagna et al., 2014; Marchitto et al., 2018), which could be exacerbated during periods of thermal stress. The Li/Mg-SST anomalies were especially low during some years which resulted in a larger RMSE 0.67±0.65 °C (Table 3) compared to Sr/Ca-SST and AVHRR-OISSTv2, ERSSTv4, as well as local air temperatures. A potential limitation for the use of Li/Mg as SST proxy is the small number of studies to date reporting Li/Mg-SST relationships (regression slopes) in tropical *Porites* corals (Hathorne et al., 2013; Montagna et al., 2014; D'Olivo & McCulloch, 2017; Marchitto et al., 2018; D'Olivo et al., 2018). For example, applying the mean slope of -0.049 mmol/mol per °C for marine calcifiers reported in Montagna et al. (2014) to our Li/Mg data would lead to significant overestimations of SST anomalies, hence even larger cold biases. The mean Sr/Ca-SST relationship of -0.060 mmol/mol per °C is, on the other hand, far better constrained by a much larger number of studies (e.g. Corrège 2006; De Long et al., 2012; Pfeiffer et al., 2017). In particular, EU3 Li/Mg was most likely affected by uncertainties in the incorporation of Mg and Li into the skeleton while EU2 Li/Mg showed no irregularities. Interestingly on a seasonal scale, Li/Ca and Mg/Ca in EU3 showed the expected negative correlation; however, on interannual to

485 decadal scales these ratios were positively correlated. This perhaps reflects an "extreme"
486 example of growth effects on Li and Mg unrelated to temperature (e.g. the effect of cation
487 entrapment and heterogeneous distribution in the centres of calcification; Montagna et al.,
488 2014; Marchitto et al., 2018). In most cases calculating Li/Mg cancels out this effect by
489 leaving SST as the main controlling parameter; however, in core EU3 this appears not to be
490 as effective, leading to slightly lower correlation of Li/Mg with SST compared to Sr/Ca with
491 SST. Careful inspection of the sampling path along the major growth axes revealed that a
492 potential cause for discrepancies in Li/Ca and Mg/Ca affecting Li/Mg might be due to
493 suboptimal sampling along parallel growth axes. The overlap period of 2003 to 2012 was
494 sampled continuously in both cores without switch in growth axis, showing an excellent
495 agreement between cores including Li/Ca ($r=0.57$, $p<0.001$, $N=54$) and Mg/Ca ($r=0.58$,
496 $p<0.001$, $N=54$). Prior to 2003, core EU3 was sampled along three different growth axes
497 (1970 to 1982, 1983 to 1996 and 1996 to 2002) orientated at an angle along the core length.
498 Although all axes showed optimal growth orientations, the Li/Ca ratios in EU3 deviated from
499 the trends shown in Mg/Ca, Sr/Ca and Li/Mg. The importance of optimal sampling along
500 continuous main growth axes for optimal TE ratios and stable isotope determinations has
501 been shown in several recent studies (e.g. De Long et al., 2012; Zinke et al., 2016), which
502 also appears to be the case for the Li/Mg proxy. This sensitivity of the Li and Mg proxies in
503 core EU3, identified as *P. solida*, could also reflect a species due to slight differences in their
504 calcification strategies. For example, D'Olivo *et al*., (2018) showed a deviation for *Porites*
505 *solida* corals from other massive *Porites* species in the relationships between Sr/Ca and
506 Li/Mg with temperature. However, this requires further investigations as this is the first long-
507 term (multi-decadal) reconstruction based on Porites corals. Despite these uncertainties
508 Li/Mg was overall the second-best performing proxy in this study with the detrended Li/Mg
509 data showing an excellent agreement with the instrumental SST and Sr/Ca data. Furthermore,
510 the interannual and decadal SST variations as well as spatial correlation patterns in the Li/Mg
511 appeared not to have been affected and can be interpreted with high confidence as indicated
512 by our field correlations. Overall the results from this study confirms that Sr/Ca and Li/Mg
513 SST proxies are the most reliable proxies to date and in combination can provide with greater
514 confidence, more reliable SST reconstructions (D'Olivo et al., 2018).

515 **4.2 Regional and large-scale climate teleconnections**

516 The spatial correlations between Europa composite data and global SST data indicated a
517 strong response to local variability in the Mozambique Channel at the latitude between 15 °S

518 and 30 °S. The pattern of spatial correlation also suggested teleconnections with the
519 northern/eastern Indian Ocean, the southeastern Pacific and the tropical Atlantic. ENSO
520 influence in the instrumental data was weak and absent in our proxy records. Only the
521 warmest years (summer maxima) of the Europa composite time series corresponded with
522 strong El Niño (1998, 2010) and La Niña (1999, 2000, 2011) events, as attested for example
523 by the high coral mortality reported from 1998 (Quod & Garnier 2004) and the moderate
524 coral bleaching observed in 2011 (Guillaume & Bruggemann 2011). Local air temperatures
525 and AVHRR-OISSTv2 anomalies indicated other warm years (>0.5 °C) corresponding to El
526 Niño years (1983, 1988, 1991/92), La Niña years (1989, 1996) and ENSO neutral years
527 (1981, 2007, 2012/13). The majority of these lower magnitude warm events were also
528 recorded in the coral proxy time series. Overall these results suggest a weak or variable
529 impact of ENSO around Europa.

530 Perhaps the most interesting and to some extent unexpected relationship of our study region
531 was found with the northern tropical Atlantic (5 °N to 20 °N, 30 °W to 80 °W), a region that
532 corresponds with the main development region for Hurricanes in the tropical Atlantic
533 (Knutson et al., 2010). This region also has strong relationships with the AMO, which is the
534 leading mode of multi-decadal variability in the northern Atlantic and thought to be driven by
535 Atlantic Meridional Ocean Circulation (AMOC) variability (e.g. Schlesinger & Ramankutty,
536 1994; Kerr, 2000; Knight et al., 2005). Our coral-based SST reconstructions and satellite data
537 revealed a strong relationship with both the Tropical North Atlantic (TNA; Enfield et al.,
538 1999) and North Tropical Atlantic indices (NTA; Penland & Matrosova, 1998) as well as the
539 AMO since at least 1970 (Table 4). However, the ERSSTv4 for Europa showed non-
540 significant correlations with the AMO, while the relationship with the northern tropical
541 Atlantic SST was robust. The exact mechanism for this teleconnection between the
542 Mozambique Channel and the tropical Atlantic remains elusive. We speculate that
543 atmospheric processes in response to AMO, tropical Atlantic or Indo-Pacific variability
544 might be controlling this relationship since all correlated regions lie within or near trade wind
545 convergence zones (the Intertropical Convergence Zone) where atmospheric circulation
546 associated with deep convection controls underlying SST (Schott et al., 2009; Xie et al.,
547 2010; Marshall et al., 2014; Green et al., 2017; Koseki & Bhatt, 2018). Wind-driven
548 upwelling controls the regions with positive correlations (negative with the geochemical
549 proxies) in the northern and eastern Indian Ocean, the northern South China Sea and the
550 southeastern Pacific (Schott et al., 2009; Xie et al., 2009; Varela et al., 2015; Sydeman et al.,

2014). The strongest resemblance to an atmospheric pattern driving the observed SST pattern, including teleconnections with the Mozambique Channel, was found with the Pacific/North American (PNA) pattern (Trenberth et al., 1998). The PNA is one of the strongest modes of low-frequency atmospheric variability in the Northern Hemisphere with an equivalent Pacific/South American pattern in the Southern Hemisphere (Mo & Peagle, 2001; Irving & Simmonds, 2016). The PNA/PSA pattern is strongly influenced by ENSO and the Pacific Decadal Oscillation (PDO; Mantua et al., 1997), tending towards being in its positive phase during El Niño and negative phase during La Niña (Rodionov & Assel, 2001). The importance of atmospheric processes for Indo-Pacific climate teleconnections emanating from the Pacific PNA and PSA patterns has been documented in several studies (Rodionov & Assel, 2001; Dai et al., 2017). The Mozambique Channel and adjacent southern Africa are both impacted by PNA/PSA variability (Blamey et al., 2018). Therefore, our spatial correlation between the TNA, NTA, PNA and global SST point towards tropical-extratropical atmospheric forcing of the observed SST teleconnection patterns in our study.

5 Conclusions

A comparison of multiple trace element ratios in two *Porites* cores from Europa (southern Mozambique Channel) indicated that Sr/Ca was the most robust paleothermometer analysed. In addition to Sr/Ca, Li/Mg and their combination showed great potential for improved higher confidence multi-element SST reconstructions. The SST over the last 42 years (1970 to 2012) was dominated by interannual variability with a warming trend of 0.58 ± 0.1 °C in Sr/Ca-SST in close agreement with instrumental data (0.47 ± 0.07 °C). Li/Mg and the combination of Li/Mg and Sr/Ca showed unrealistically large warming trends, most probably caused by uncertainties around Li/Ca and Mg/Ca incorporation with marginally different uptake mechanisms for these trace elements. However, detrended data from Sr/Ca, Li/Mg and the combination of Li/Mg and Sr/Ca agreed well with each other and with regional instrumental SST and local air temperature. Spatial correlations between detrended Sr/Ca, Li/Mg and combined proxies with instrumental SST at Europa revealed robust correlations with local climate variability in the Mozambique Channel and teleconnections to regions in the tropical Atlantic Ocean, Indian Ocean and southeastern Pacific where surface wind variability appeared to dominate the underlying SST. Of particular interest is the strong correlation found between the proxy and instrumental SST records with the northern tropical Atlantic SST. Only a weak correlation was found with ENSO, with recent warm anomalies in the geochemical proxies coinciding with strong El Niño or La Niña. We identified the PNA

584 atmospheric pattern, which develops in the Pacific in response to ENSO, and the tropical
585 North Atlantic SST as the most likely causes of the observed teleconnections with the
586 Mozambique Channel SST. In conclusion, the Europa *Porites* sp. geochemical records
587 highlight the great potential of Sr/Ca and Li/Mg ratios as accurate, reliable high-resolution
588 climate archives for the tropical oceans.

589 **6 Data availability**

590 Trace element data will be made publically available on the NOAA's WDC paleoclimate data
591 server https://www.ncdc.noaa.gov/data-access/paleoclimatology-data/datasets.

592

593 **7 Author contribution**

594 JZ, MMMG, JHB, JCG and JPD designed the study and lead the writing of the manuscript.
595 MMMG provided the samples, JZ, JPD and MMM organised and performed the trace
596 element analysis, while JML did the coral densitometry measurements. All co-authors
597 contributed to analysis and writing of the manuscript.

598

599 **8 Acknowledgments**

600 The scientific expedition *ORCIE 2013* conducted by Mireille Guillaume benefited from
601 financial support from CNRS-INEE for the inter-organism program *îles Eparses* and from the
602 *Association Française des Plongeurs Scientifiques* (COLIMPHA). Authorisations for diving
603 around Europa and a CITES export permit (# FR1398400001-E) were provided by the *Terres*
604 *australes et antarctiques françaises* (TAAF) administration. The assistance of the skipper J-B
605 Galves and crew of the vessel *Inventive* is gratefully acknowledged. We further thank the
606 professional divers Jean-Patrick Rousse and Erwan Meyer for their efficient help in coring
607 the coral colonies, and the Division Technique from CNRS-INSU, especially Michel Calzas,
608 Christine Drezen and Christophe Guillerm, for sharing the temperature records of the RBR
609 gauges, that were deployed and retrieved by Jean-Patrick Rousse. MMMG also received
610 funds from the MNHN/UMR BOrEA and from the ANR-STORISK project (No.ANR-15-
611 CE03-0003) for element analysis. We thank Kai Rankenburg from The University of Western
612 Australia Advanced Geochemical Facility for Indian Ocean Research for support in trace
613 element measurements. Météo-France is acknowledged. Research conducted at UWA was
614 supported by the Australian Research Council through the Centre of Excellence for Coral
615 Reef Studies (CE140100020), and a Laureate Fellowship awarded to Malcolm McCulloch
616 (FL120100049).

617 **9 References**

Alibert, C. and McCulloch M. T.: Strontium/calcium ratios in modern *Porites* corals from the Great Barrier Reef as a proxy for sea surface temperature: calibration of the thermometer and monitoring of ENSO, Paleoceanography, 12, 345–363,1997.

Angell, J. K.: Variation in global tropospheric temperature after adjustment for the EI Niño influence, 1958-1989, Geophys. Res. Leu., 17,1097-1110, 1990.

Banzon, V., Smith, T. M., Chin, T. M., Liu, C., and Hankins, W.: A long-term record of blended satellite and in situ sea-surface temperature for climate monitoring, modeling and environmental studies. Earth Syst. Sci. Data, 8, 165–176, 2016.

Banzon, V. F., Reynolds, R. W., Stokes, D. and Xue, Y.: A 1/4° spatial resolution daily sea surface temperature climatology based on a blended satellite and in situ analysis. Journal of Climate, 27, 8221–8228, 2014.

Barruol G., Davy C., Fontaine F.R., Schlindwein V., Sigloch K.: Monitoring austral and cyclonic swells in the "Iles Eparses (Mozambique channel) from microseismic noise. Acta Oecologica 72, 120-128, 2016.

Battistini R, Lalou C, Elbez G. : Datation par la méthode ^{230}Th ^{234}U du Pléistocène moyen marin de Madagascar et des îles voisines. C R somm Soc géol France 5: 201pp, 1976.

Beal, L. M., De Ruijter, W.P.M., Biastoch, A., Zhan, R. and SCOR/WCRP/IAPSO Working Group 136: On the role of the Agulhas system in ocean circulation and climate. *Nature* 472, 429-436, 2011.

Blamey, R. C., Kolusu, S. R., Mahlalela, P., Todd, M. C., Reason, C. J. C.: The role of regional circulation features in regulating El Niño climate impacts over southern Africa: A comparison of the 2015/2016 drought with previous events. Intrenational Journal of Climatology, doi:10.1002/joc.5668, 2018.

Brewin, R.J.W., de Mora, L., Billson, O., Jackson, T., Russell, P., Brewin, T.G., Shutler, J.D., Miller, P.I., Taylor, B.H., Smyth, T.J. and Fishwick, J.R.: Evaluating operational AVHRR sea surface temperature data at the coastline using surfers. Estuarine, Coastal and Shelf Science 196, 276-289, 2017.

Cohen, A. L., K. E. Owens, G. D. Layne, and Shimizu N.: The effect of algal symbionts on the accuracy of Sr/Ca paleotemperatures from coral, Science, 296(5566), 331–333, doi:10.1126/science.1069330, 2002.

Corrège T.: Sea surface temperature and salinity reconstructions from coral geochemical tracers. Palaeogeogr Palaeoclimatol Palaeoecol 232:408–428, 2006.

DeLong, K. L., Quinn, T. M., Taylor, F. W., Shen, C.-C., and Lin, K.: Improving coral-base paleoclimate reconstructions by replicating 350 years of coral Sr/Ca variations, Palaeogeogr., Palaeocl., 373, 6–24, 2012.

DeLong, K. L., Quinn, T. M. & Taylor, F. W.: Reconstructing twentieth-century sea surface temperature variability in the southwest Pacific: A replication study using multiple coral Sr/Ca records from New Caledonia. Paleoceanography 22, PA4212, 2007.

D'Olivo, J. P., Sinclair, D. J., Rankenburg, K., McCulloch, M. T.: A universal multi-trace element calibration for reconstructing sea surface temperatures from long-lived Porites corals: Removing 'vital-effects'. Geochimica et Cosmochimica Acta 239, 109–135, 2018.

De Ruijter, W.P.M., Ridderinkhof, H., Lutjeharms, J.R.E., Schouten, M.W., Veth, C.: Observations of the flow in the Mozambique Channel, Geophys. Res. Lett. 29 (10) 140–142, 2002.

Enfield, D.B., Mestas, A.M., Mayer, D.A. and Cid-Serrano. L.: How ubiquitous is the dipole relationship in tropical Atlantic sea surface temperatures? JGR-O, 104, 7841-7848, 1999.

Gaetani, G. A., Cohen, A. L., Wang, Z., and Crusius, J.: Rayleigh-based, multi-element coral thermometry: A biomineralization approach to developing climate proxies, Geochim. Cosmochim. Acta, 75, 1920–1932, doi:10.1016/j.gca.2011.01.010, 2011.

Gaetani, G. A., and Cohen, A. L.: Element partitioning during precipitation of aragonite from seawater: A framework for understanding paleoproxies, Geochim. Cosmochim. Acta, 70(18), 4617–4634, doi:10.1016/j.gca.2006.07.008, 2006.

Green, B., Marshall, J. and Donohoe, A.: Twentieth century correlations between extratropical SST variability and ITCZ shifts, Geophys. Res. Lett., 44, 9039–9047, 2017.

Guillaume M.M.M. & Bruggemann J.H.: Coral bleaching in 2011 in NTA's of the southern Mozambique Channel (Europa and Bassas da India). 7th Western Indian Ocean Marine Science Association scientific symposium. Mombasa, Kenya, 24-29/10 (oral. comm.), 2011.

Guillaume M.M.M., Reyss J.-L., Pirazzoli P.A. and Bruggemann J.H.: Tectonic stability since the last interglacial offsets the Glorieuses Islands from the nearby Comoros archipelago. *Coral Reefs* 32: 719-726. DOI:10.1007/s00338-012-1006-9, 2013.

Hartnady C.J.H.: Uplift, faulting, seismicity, thermal spring and possible incipient volcanic activity in the Lesotho-Natal region, SE Africa: The Quathlamba Hotspot hypothesis. Tectonics 4: 371-377, 1985.

Hathorne E. C., Felis T., Suzuki A., Kawahata H. and Cabioch G.; Lithium content of the aragonitic skeletons of massive *Porites* corals: a new tool to reconstruct tropical sea surface temperatures. *Paleoceanography*, 28, 143–152, 2013.

Hennekam, R., Zinke, J., ten Have, M., Brummer, G.J.A. and Reichart, G.-J.: Cocos (Keeling) corals reveal 200 years of multi-decadal modulation of southeast Indian Ocean hydrology by Indonesian Throughflow. Paleoceanography and Paleoclimatology, 33, 48-60, doi: 10.1002/2017PA003181, 2018.

Irving, D., and Simmonds, I.: A new method for identifying the Pacific–South American pattern and its influence on regional climate variability. J. Climate, 29, 6109–6125, 2016.

Kaplan, A., Cane, M. A., Kushnir, Y., Clement, A. C., Blumenthal, M. B., Rajagopalan, B. Ana of global sea surface temperature 1856-1991, J. Geophys. Res., 103, 18567-18589, 1998.

Kerr, R. A. A.: North Atlantic Climate Pacemaker for the Centuries. Science 288, 1984–1986, 2000.

Knight, J. R., Allan, R. J., Folland, C. K., Vellinga, M. & Mann, M. E.: A signature of persistent natural thermohaline circulation cycles in observed climate. Geophysical Research Letters 32, doi: 10.1029/2005gl024233, 2005.

Knutson, T. R., McBride, J. L., Chan, J., Emanuel, K., Holland, G., Landsea, C., Held, I., Kossin, J. P., Srivastava, A. K. and Sugi, M.: Tropical cyclones and climate change. Nat. Geosci. 3, 157–163, 2010.

Koseki, S. and Bhatt, B. C.: Unique relationship between tropical rainfall and SST to the north of the Mozambique Channel in boreal winter. Int. J. Climatol. 38, c378-c387, doi:10.1002/joc.5378, 2018.

Liu, W., Huang, B., Thorne, B.W., Banzon, V. F., Zhang, H.-M., Freeman, E., Lawrimore, J., Peterson, T. C., Smith, T. M., Woodruff, S. D.: Extended Reconstructed Sea Surface Temperature Version 4 (ERSST.v4): Part II. Parametric and Structural Uncertainty Estimations. Journal of Climate 28, 931-951, 2015.

Mantua, N. J., Hare, S. R., Zhang, Y., Wallace, J. M. and Francis, R. C.: A Pacific interdecadal climate oscillation with impacts on salmon production. Bull. Am. Meteorol. Soc., 78(6), 1069–1079, 1997.

Marchitto, T. M., Bryan, S. P., Doss, W., McCulloch, M. T., & Montagna, P.: A simple biomineralization model to explain Li, Mg, and Sr incorporation into aragonitic foraminifera and corals. *Earth and Planetary Science Letters*, 481, 20-29. DOI: 10.1016/j.epsl.2017.10.022, 2018.

Marshall, J., Donohoe, A., Ferreira, D., and McGee, D. The ocean's role in setting the mean position of the Inter-Tropical Convergence Zone, Clim. Dyn., 42, 1967–1979, 2014.

Montagna, P., McCulloch, M. T., Douville, E., Lopez Correa, M., Trotter, J., Rodolfo-Metalpa, R., Dissard, D., Ferrier-Pages, C., Frank, N., Freiwald, A., Goldstein, S., Mazzoli, C., Reynaud, S., Rüggeberg, A., Russo, S., Taviani, M.: Li/Mg systematics in scleractinian corals: Calibration of the Thermometer. *Geochimica et Cosmochimica Acta*, 132, 288–310, 2014.

Mo, K. C., and Paegle, J. N.: The Pacific South–American modes and their downstream effects. Int. J. Climatol., 21, 1211–1229, 2001.

Nagtegaal R., Grove C.A., Kasper S., Zinke J., Boer W., Brummer G.J.A.: Spectral luminescence and geochemistry of coral aragonite: effects of whole-core chemical treatments. Chemical Geology 318-319, 6-15, 2012.

Okai, T., Suzuki, A., Kawahata, H., Terashima, S. & Imai, N.: Preparation of a new Geological Survey of Japan geochemical reference material: Coral JCp-1. Geostandard. Newslett. 26, 95–99, 2002.

Penland, C., and Matrosova, L.: Prediction of tropical Atlantic sea surface temperatures using Linear Inverse Modeling, Journal of Climate 11, 483-496, 1998.

Pfeiffer, M., Zinke, J., Dullo, W.-C., Timm, O., Cahyarini, S.Y., Latif, M. and Weber, M. E.: Indian Ocean corals reveal crucial role of World War II bias for twentieth century warming estimates. Scientific Reports 7, 14434, doi:10.1038/s41598-017-14352-6, 2017.

Pfeiffer, M., Dullo, W.C., Zinke, J. and Garbe-Schoenberg, D.: Three monthly coral Sr/Ca records from the Chagos Archipelago covering the period of 1950 to 1995.: Reproducibility and implications for quantitative reconstructions of sea surface temperature variations. International Journal of Earth Sciences 98, Special Volume, doi:10.007/s00531-008-0326-z, 2009.

Quod J.-P. & Garnier R.: A preliminary assessment of the coral reefs of Europa (Mozambique channel). Reef Encounter 32 , 23-25, 2004.

Reynolds, R. W., Smith, T. M., Liu, C., Chelton, D. B., Casey, K. S. and Schlax, M. G.: Daily high-resolution-blended analyses for sea surface temperature. Journal of Climate, 20, 5473–5496, 2007.

Riodionov, S., Assel, R.: A New Look at the Pacific/North American Index. Geophysical Research Letters 28 (8), 1519-1522, 2001.

Schouten, M.W., De Ruijter, W.P.M., Van Leeuwen, P.J., Dijkstra, H.A.: An oceanic teleconnection between the equatorial and southern Indian Ocean, Geophys. Res. Lett. 29 (16), 9–62, 2002.

Schlesinger, M. E. & Ramankutty, N.: An oscillation in the global climate system of period 65–70 years. Nature 367, 723–726, 1994.

Schott, F. A., Xie, S. P., McCreary Jr., J. P.: Indian Ocean circulation and climate variability. Review in Geophysics, 47, RG1002, doi:10.1029/2007RG000245, 2009.

Smit, A.J., Roberts, M., Anderson, R.J., Dufois, F., Dudley, S.F.J., Bornman, T.G., Olbers, J. and Bolton, J.J.: A Coastal Seawater Temperature Dataset for Biogeographical Studies: Large Biases between In Situ and Remotely-Sensed Data Sets around the Coast of South Africa. PLOS ONE 8, e81944, 2013.

Smith, S. V., Buddemeier, R. W., Redalje, R. C. and Houck, J. E.: Strontium-calcium thermometry in coral skeletons, Science, 204, 404-406, 1979.

Swart, N. C., Lutjeharms, J. R. E., Ridderinkhof, H. and de Ruijter, W. P. M.: Observed characteristics of Mozambique Channel eddies. Journal of Geophysical Research115, C09006, doi:10.1029/2009JC005875, 2010.

Sydeman, W. J., García-Reyes, M., Schoeman, D. S., Rykaczewski, R. R., Thompson, S., Black, B. A. and Bograd S. J.: Climate change and wind intensification in coastal upwelling ecosystems. Science 345, 77, 2014.

Testut L., Duvat V., Ballu V., Fernandes R.M.S., Pouget F., Salmon C., Dyment J.: Shoreline changes in a rising sea level context: The example of Grande Glorieuse, Scattered Islands, Western Indian Ocean. Acta Oecologica 72: 110-119, 2016.

Timmermann, A., Si, A., Kug, J. S. et al. El Nino-Southern Oscillation complexity. Nature 559, 535-545, 2018.

Trenberth, K. E., Branstator, G. W. , Karoly, D., Kumar, A., Lau, N. and Ropelewski, C: Progress during TOGA in understanding and modeling global teleconnections associated with tropical sea surface temperatures. J. Geophys. Res., 103, 14291–14324, 1998.

Thompson, D. W. J., Kennedy, J. J., Wallace, J. M. & Jones, P. D.: A large discontinuity in the mid-twentieth century in observed global-mean surface temperature. Nature 453, 646–649, 2008.

Trouet, V. and van Oldenborgh, G.J.: KNMI Climate Explorer: a web-based research tool for high-resolution paleoclimatology. Tree Ring Research, 69, 1, 3-13, 2013.

Van den Berg, M.A., Morris, T., Roberts, M. J. Long-term temperature monitoring in the Mozambique Channel. Conference abstract, 5th Western Indian Ocean Marine Science Organisation Symposium, 22-26th of October 2007, Durban, South Africa, (oral communic.), 2007.

Varela, R., Álvarez, I., , Santos, F., deCastro, M., Gómez-Gesteira, M.: Has upwelling strengthened along worldwide coasts over 1982-2010? Scientific Reports 5, 10016, doi:10.1038/srep10016, 2015.

Woodruff, S.D., Worley, S. J., Lubker, S. J., Ji, Z., J. Freeman, E., Berry, D. I., Brohan, P., Kent, E. C., Reynolds, R. W., Smith, S. R.. and Wilkinson, C.: ICOADS Release 2.5: Extensions and enhancements to the surface marine meteorological archive. *Int. J. Climatol.*, 31, 951-967, 2011.

Xie, S. P., Deser, C., Vecchi, G., Ma, J., Teng, H., Wittenberg, A. T.: Global warming pattern formation: Sea surface temperature and rainfall. Journal of Climate 23, 966-986, 2010.

Zinke, J., Reuning, L., Pfeiffer, M., Wassenburg, J.A., Hardman, E., Jhangeer-Khan, R., Davies, G.R., Ng, C.K.C., Kroon, D.: A sea surface temperature reconstruction for the southern Indian Ocean trade wind belt from corals in Rodrigues Island (19S, 63E). Biogeosciences 13, 5827-5847, 2016.

Zinke, J., Hoell, A., Lough, J., Feng, M., Kuret, A., Clarke, H., Ricca, V., McCulloch, M.T.: Coral record of southeast Indian Ocean marine heatwaves with intensified Western Pacific temperature gradient. Nat. Commun. 6:8562 doi: 10.1038/ncomms9562, 2015.

Zinke, J., Timm, O., Pfeiffer, M., Dullo, W.-Chr., Kroon, D. and Thomassin, B. A.: Mayotte coral reveales hydrological changes in the western Indian between 1865 to 1994. Geophysical Research Letters 35, L23707, doi:10.1029/2008GL035634, 2008.

Zinke, J., Dullo, W.-Chr., Heiss, G. A. & Eisenhauer, A.: ENSO and subtropical dipole variability is recorded in a coral record off southwest Madagascar for the period 1659 to 1995. Earth and Planetary Science Letters 228 (1-2), 177-197, 2004.

Biogeosciences Discuss., https://doi.org/10.5194/bg-2018-441
Manuscript under review for journal Biogeosciences
Discussion started: 16 October 2018

630 **Tables**

Location	Latitude (S)	Longitude (E)	Depth (m)	Core #	Length	Collection dates
North Reef	22°19.839	40°21.758	12.80	EU-2	105	2/5/2013
North-East Reef	22°20.119	40°23.333	12.00	EU-3	136	3/5/2013

Table 1 – Coral core GPS locations from Europa, water depth, core name, core length and collection dates.

Biogeosciences Discuss., https://doi.org/10.5194/bg-2018-441
Manuscript under review for journal Biogeosciences
Discussion started: 16 October 2018

core	proxy	SST product	slope	Conf. interval	intercept	Conf. interval	r^2	r^2 adj.	SSE	RMSE	DoF	Period
EU2	Sr/Ca	AVHRR-OISSTv2	-0.045	0.0031	10.241	0.083	0.093	0.94	0.021	0.02	53	2003-2012
		ERSSTv4	-0.051	0.0038	10.395	0.100	0.93	0.93	0.023	0.021	53	2003-2012
	Li/Mg	AVHRR-OISSTv2	-0.045	0.0033	2.672	0.088	0.93	0.93	0.023	0.021	53	2003-2012
		ERSSTv4	-0.051	0.0044	2.815	0.115	0.91	0.91	0.030	0.024	53	2003-2012
EU3	Sr/Ca	AVHRR-OISSTv2	-0.04	0.0031	9.974	0.083	0.92	0.92	0.020	0.019	53	2003-2012
		ERSSTv4	-0.046	0.0035	10.117	0.093	0.92	0.92	0.020	0.019	53	2003-2012
	Li/Mg	AVHRR-OISSTv2	-0.052	0.007	2.739	0.200	0.78	0.78	0.119	0.047	53	2003-2012
		ERSSTv4	-0.060	0.009	2.927	0.226	0.78	0.78	0.119	0.047	53	2003-2012
	Sr/Ca	AVHRR-OISSTv2	-0.042	0.002	10.049	0.064	0.86	0.86	0.138	0.027	184	1981-2012
		ERSSTv4	-0.048	0.002	10.191	0.058	0.88	0.88	0.179	0.027	252	1970-2012
	Li/Mg	AVHRR-OISSTv2	-0.057	0.004	2.898	0.117	0.77	0.77	0.452	0.049	184	1981-2012
		ERSSTv4	-0.064	0.004	3.076	0.108	0.78	0.78	0.612	0.049	252	1970-2012

Table 2 – Linear optimal least squares regression equations for core EU2 and EU3 Sr/Ca and Li/Mg ratios with AVHRR-OI SSTv2 and ERSSTv4. Conf. interval= 95% confidence interval of the regression slopes and intercepts; r^2 adj.= r^2 adjusted; SSE= Standard Error; RMSE= Root Mean Square Error; DoF= degrees of freedom.

Biogeosciences Discuss., https://doi.org/10.5194/bg-2018-441
Manuscript under review for journal Biogeosciences
Discussion started: 16 October 2018

	Individual proxies RMSE and SD					
Core ID	**Sr/Ca**	**Li/Mg**	**Mg/Ca**	**Li/Ca**	**Sr/Ca-Li/Mg**	**Period**
EU2	0.38±0.26	0.36±0.30	1.13±0.89	0.58±0.50	0.32±0.25	2003-2012
EU3	0.41±0.29	0.90±0.99	1.79±1.76	1.65±1.22	0.60±0.57	2003-2012
EU3	0.55±0.36	0.74±0.66	1.33±1.18	1.41±0.98	0.62±0.50	1981-2012
Avg. all	**0.45**	**0.67**	**1.42**	**1.21**	**0.51**	1981-2012
S.D. all	**0.30**	**0.65**	**1.28**	**0.90**	**0.44**	1981-2012

Table 3 – Root mean square error (RMSE) and their standard deviation (S.D.) for trace element ratios against AVHRR-OISSTv2 for individual trace element ratios and Sr/Ca-Li/Mg combination. Period used for calculation of RMSE indicated in last column.

Biogeosciences Discuss., https://doi.org/10.5194/bg-2018-441
Manuscript under review for journal Biogeosciences
Discussion started: 16 October 2018

	Northern Tropical Atlantic SST	AMO Index	TNA/NTA	Niño3.4
#EU-AVHRR-OISSTv2	0.59***	0.37**	0.55***/ 0.53***	0.47** (FMA)
^EU-ERSSRv4	0.37**	0.18	0.34**/ 0.36**	0.34** (JFMA)
^EU-composite Sr/Ca SST anomalies	0.61***	0.46***	0.53***/ 0.45**	-
^EU-composite Li/Mg SST anomalies	0.55***	0.54***	0.40** / 0.32*	-
^EU-composite Sr/Ca-Li/Mg SST anomalies	0.60***	0.52***	0.47***/ 0.39**	-

#1981-2013; ^1970-2013; *=90%, **=95%, ***=99% significance

Table 4 – Linear correlation of detrended, mean annual instrumental and coral proxy-based SST for Europa (EU) with northern tropical Atlantic SST, the AMO index based on ERSSTv4, the Tropical North Atlantic (TNA; Enfield et al., 1999) and North Tropical Atlantic index (Penland & Matrosova, 1998) and the seasonal Niño3.4 index (Kaplan et al., 1998).

Biogeosciences Discuss., https://doi.org/10.5194/bg-2018-441
Manuscript under review for journal Biogeosciences
Discussion started: 16 October 2018

Figure captions

Fig. 1 Coral collection sites for cores EU2 and EU3 along the northern-northeastern reef slope of Europa and its positioning within the southern Mozambique Channel (south-west Indian Ocean).

Fig 2 Bimonthly interpolated time series of trace element/Ca proxies from cores EU2 and EU3. a) Sr/Ca, b) Li/Mg, c) Mg/Ca and d) Li/Ca.

Figure 3 – Scatter plot of bimonthly trace element ratios in cores EU2 (black dots) and EU3 (blue dots) over the full length of the records. a-c) Sr/Ca ratios vs. Li/Mg, Mg/Ca and Li/Ca, d-e) Li/Mg vs. Mg/Ca and Li/Ca and f) Li/Ca vs. Mg/Ca. The 95% prediction intervals of the regressions are indicated by red dashed (EU3) and green solid lines (EU2) and linear fits for each core with a red line. Regression equations are provided in Table S1.

Figure 4 - Linear regressions of TE/Ca proxies with AVHRR-OISSTv2 (Banzon et al., 2016) for core EU3 1981-2012 (a,c) and EU2 2003-2012 (b,d). The TE/Ca records were calibrated using the respective linear regression equations of the bimonthly correlations obtained for each of the core records from the two sites. The 95% confidence intervals of the regressions are indicated. Regression equations are provided in Table 2.

Figure 5 Absolute SST reconstructions for cores EU3 (red) and EU2 (blue) with SST residuals based on the calibration period 1981 to 2012 for a) Sr/Ca-SST, b) Li/Mg-SST and c) their combination in comparison to AVHRR-OISSTv2 (Banzon et al., 2016; black) and *in situ* SST (orange; 2009-2010). d) residuals for Sr/Ca-SST, Li/Mg-SST and their combination for cores EU2 and EU3 with respect to the AVHRR-OISSTv2 data (Banzon et al., 2016).

Figure 6 - SST anomaly reconstructions with SST residuals for a) EU composite Sr/Ca, b) EU composite Li/Mg and c) their combination for cores EU2 and EU3. d) residuals for SST anomalies of Sr/Ca-SST, Li/Mg-SST and their combination for cores EU2 and EU3 with respect to the AVHRR-OISSTv2 data (Banzon et al., 2016). Anomalies were calculated relative to the 1981 to 2010 average bimonthly seasonal cycle.

Figure 7 Comparison of coral composite Sr/Ca-SST, Li/Mg-SST and Sr/Ca-Li/Mg-SST anomaly reconstructions with air temperature from Europa Météo-France weather station data. a) Sr/Ca-SST composite, b) Li/Mg-SST composite, c) Sr/Ca-Li/Mg-SST composite, d) Europa gridded AVHRR-OISSTv2 (Banzon et al., 2016) and e) Europa gridded ERSSTv4. Anomalies were calculated relative to the 1981 to 2010 average bimonthly seasonal cycle for proxy reconstructions, instrumental SST and air temperatures.

Figure 8 - Mean annual coral growth parameters of cores EU2 and EU3 compared to coral composite Sr/Ca-SST reconstruction, AVHRR-OISSTv2 (Banzon et al., 2016) and ERSSTv4 (Liu et al., 2015). a) mean annual SST time series, b) linear extension rate, c) skeletal density and d) calcification rate.

Figure 9 - Regional comparison of Mozambique Channel ERSSTv4 anomalies for Mayotte (green), Europa (orange) and Ifaty Madagascar (blue) in a) with linear warming trends in brackets. EU Sr/Ca-SST composite anomaly compared with b) Mayotte δ^{18}O-SST anomaly (blue), c) Mayotte Sr/Ca-SST anomaly (blue), d) Ifaty δ^{18}O -SST anomaly (blue) and e) Ifaty Sr/Ca-SST anomaly (blue). Anomalies were calculated for the 1973 to 1993 reference period. Linear warming trends indicated in b) to e) for proxy-SST for individual record length with EU composite Sr/Ca-SST anomaly only indicated once in panel b. Proxy data taken from Zinke et al. (2004, 2008).

Figure 10 - Spatial correlations of proxy-based coral composite SST reconstructions with local and global AVHRR-OISSTv2 for mean annual data (Banzon et al., 2016). a) local AVHRR-OISSTv2 with global AVHRR-OISSTv2, b) local AVHRR-OISSTv2 with EU composite Sr/Ca-Li/Mg-SST, c) local AVHRR-OISSTv2 with EU composite Sr/Ca ratios and d) local AVHRR-OISSTv2 with EU composite Li/Mg ratios. Panels e and d show spatial correlations of the TNA and PNA indices with global AVHRR-OISSTv2. Only correlations with $p<0.05$ were coloured.

Biogeosciences Discuss., https://doi.org/10.5194/bg-2018-441
Manuscript under review for journal Biogeosciences
Discussion started: 16 October 2018

Figures

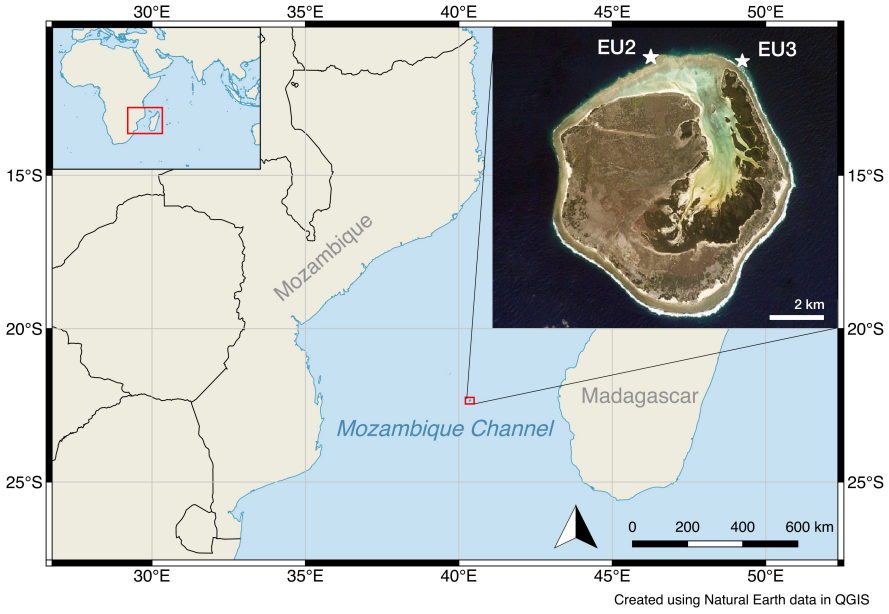

Fig. 1 Coral collection sites for cores EU2 and EU3 along the northern-northeastern reef slope of Europa and its positioning within the southern Mozambique Channel (south-west Indian Ocean).

Biogeosciences Discuss., https://doi.org/10.5194/bg-2018-441
Manuscript under review for journal Biogeosciences
Discussion started: 16 October 2018

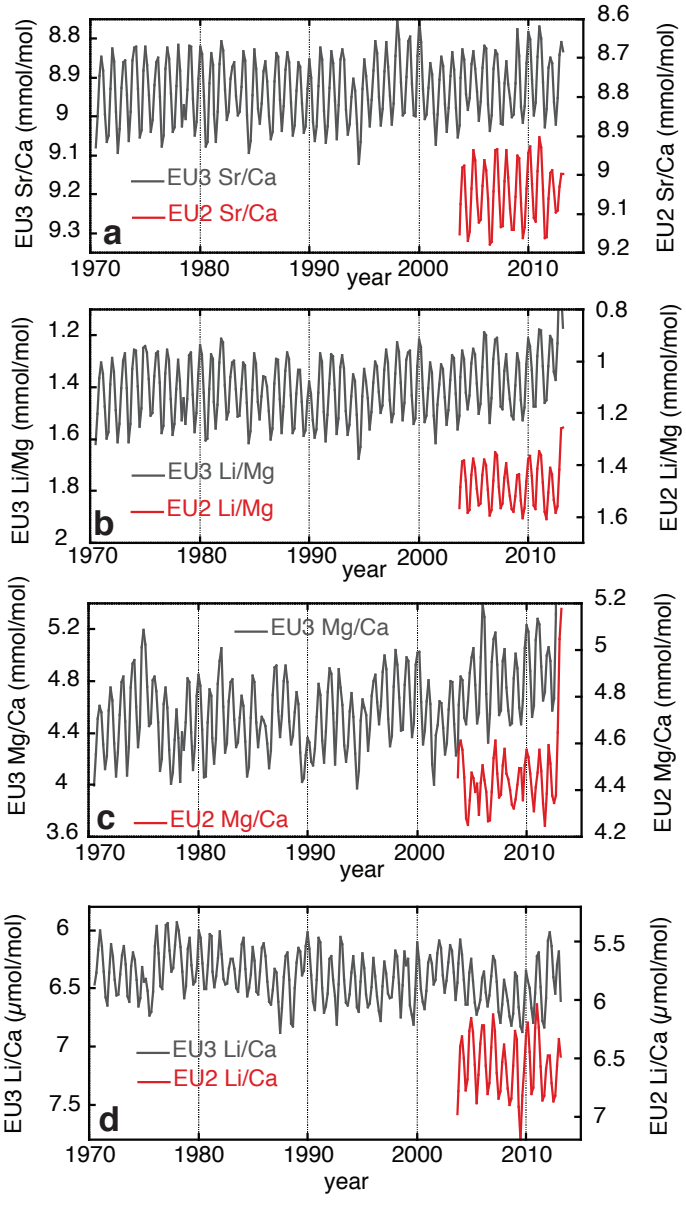

Fig 2 Bimonthly interpolated time series of trace element/Ca proxies from cores EU3 and EU2. a) Sr/Ca, b) Li/Mg, c) Mg/Ca, d) Li/Ca.

Biogeosciences Discuss., https://doi.org/10.5194/bg-2018-441
Manuscript under review for journal Biogeosciences
Discussion started: 16 October 2018

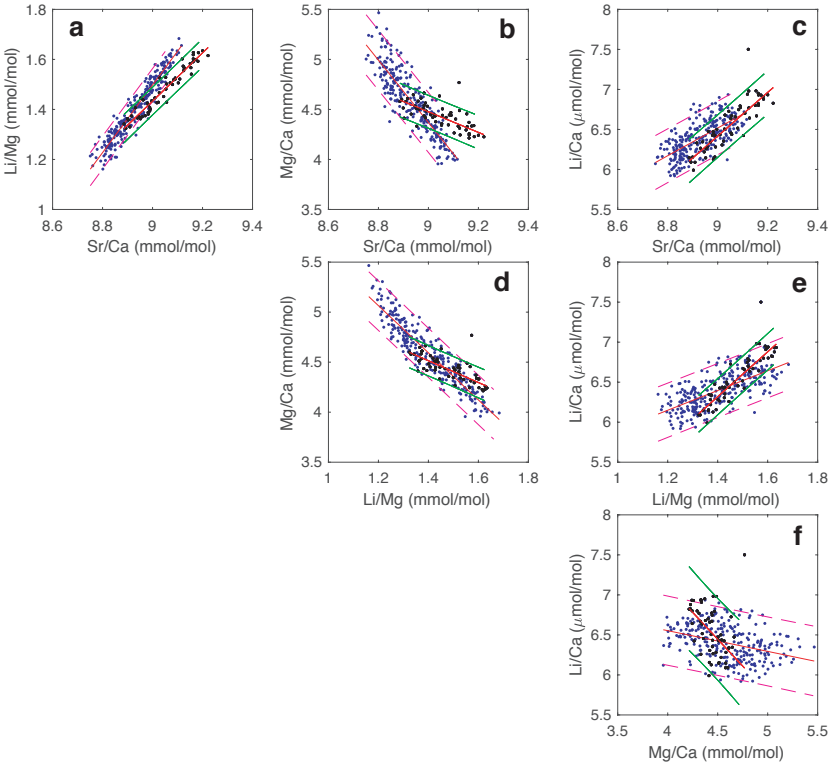

Figure 3 – Scatter plot of bimonthly trace element ratios in cores EU2 (black dots) and EU3 (blue dots) over the full length of the records. a-c) Sr/Ca ratios vs. Li/Mg, Mg/Ca and Li/Ca, d-e) Li/Mg vs. Mg/Ca and Li/Ca and f) Li/Ca vs. Mg/Ca. The 95% prediction intervals of the regressions are indicated by red dashed (EU3) and green solid lines (EU2) and linear fits for each core with a red line. Regression equations are provided in Table S1.

Biogeosciences Discuss., https://doi.org/10.5194/bg-2018-441
Manuscript under review for journal Biogeosciences
Discussion started: 16 October 2018

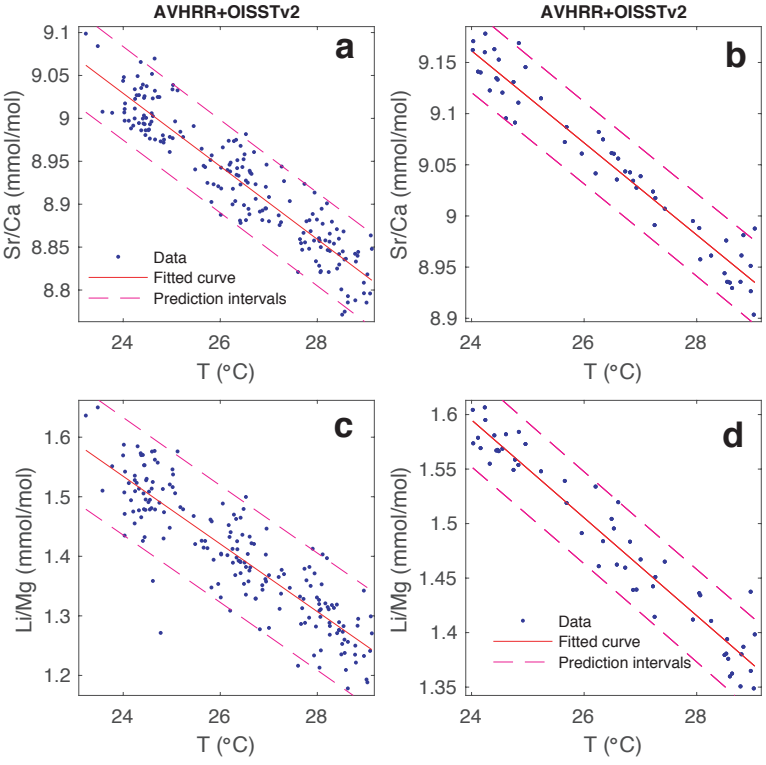

Figure 4 - Linear regressions of TE/Ca proxies with AVHRR-OISSTv2 for core EU3 1981-2012 (a,c) and EU2 2003-2012 (b,d). The TE/Ca records were calibrated using the respective linear regression equations of the bimonthly correlations obtained for each of the core records from the two sites. The 95% confidence intervals of the regressions are indicated. Regression equations are provided in Table 2.

Biogeosciences Discuss., https://doi.org/10.5194/bg-2018-441
Manuscript under review for journal Biogeosciences
Discussion started: 16 October 2018

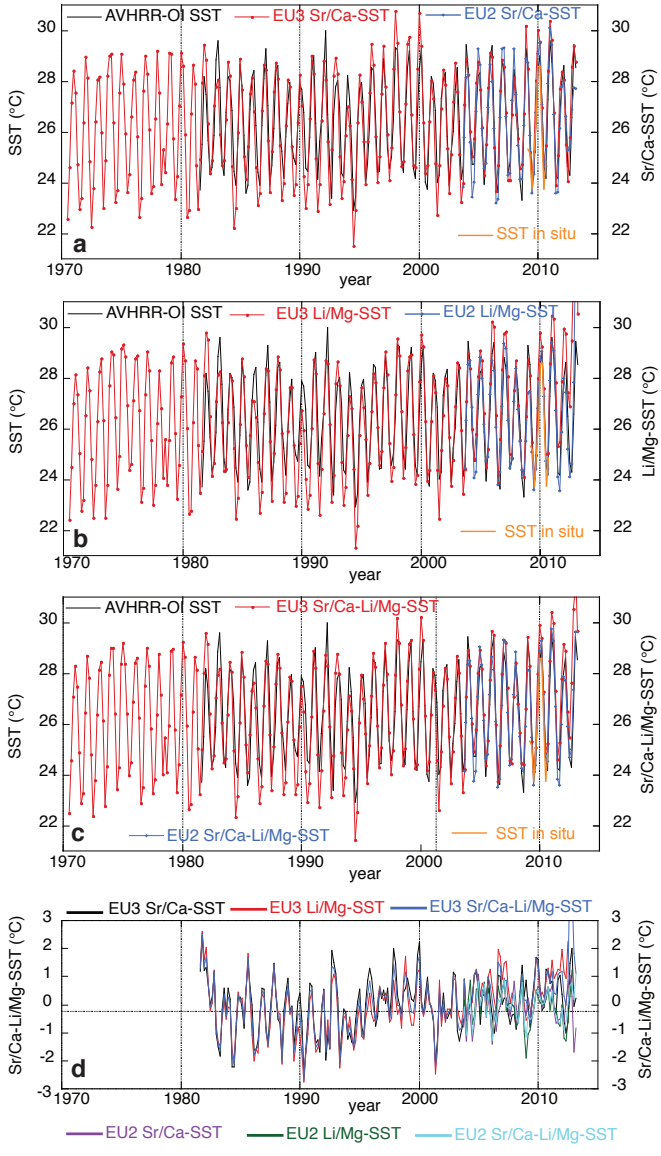

Figure 5 Absolute SST reconstructions for cores EU3 (red) and EU2 (blue) with SST residuals based on the calibration period 1981 to 2013 for a) Sr/Ca-SST, b) Li/Mg-SST and c) their combination in comparison to AVHRR-OISSTv2 (Banzon et al., 2016; black) and *in situ* SST (orange; 2009-2010). d) residuals for Sr/Ca-SST, Li/Mg-SST and their combination for cores EU2 and EU3 with respect to the AVHRR-OISSTv2 data.

Biogeosciences Discuss., https://doi.org/10.5194/bg-2018-441
Manuscript under review for journal Biogeosciences
Discussion started: 16 October 2018

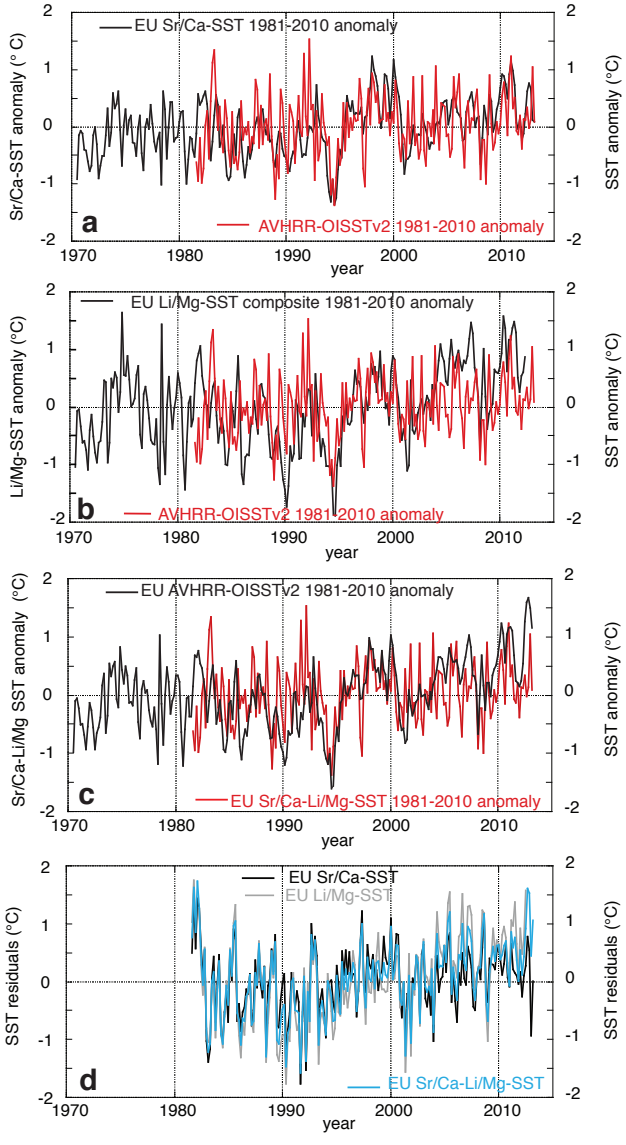

Figure 6 - SST anomaly reconstructions with SST residuals for a) EU composite Sr/Ca, b) EU composite Li/Mg and c) their combination for cores EU2 and EU3. d) residuals for SST anomalies of Sr/Ca-SST, Li/Mg-SST and their combination for cores EU2 and EU3 with respect to the AVHRR-OISSTv2 data (Banzon et al., 2016). Anomalies were calculated relative to the 1981 to 2010 average bimonthly seasonal cycle.

Biogeosciences Discuss., https://doi.org/10.5194/bg-2018-441
Manuscript under review for journal Biogeosciences
Discussion started: 16 October 2018

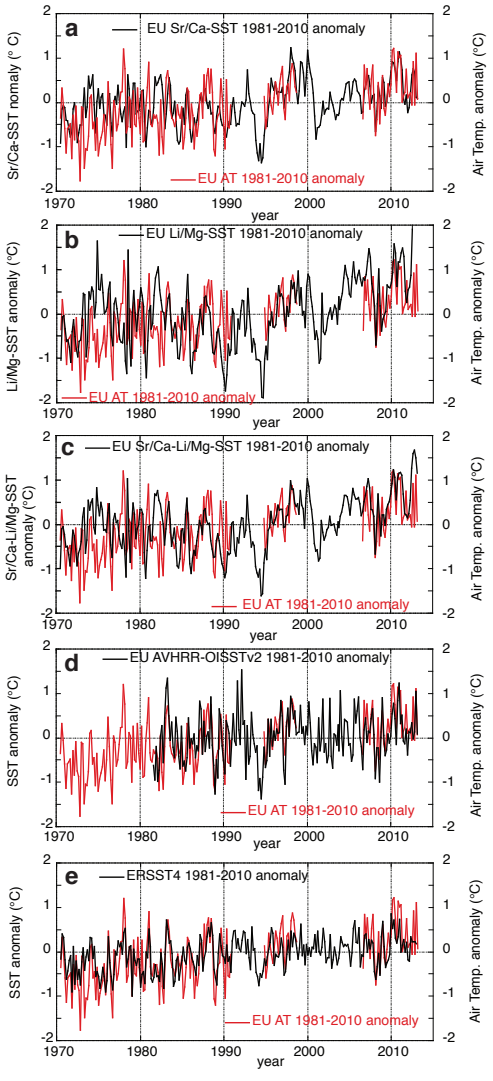

Figure 7 Comparison of Europa (EU) coral composite Sr/Ca-SST, Li/Mg-SST and Sr/Ca-Li/Mg-SST anomaly reconstructions with air temperature (AT) from Europa Météo-France weather station data. a) Sr/Ca-SST composite, b) Li/Mg-SST composite, c) Sr/Ca-Li/Mg-SST composite, d) Europa gridded AVHRR-OISSTv2 (Banzon et al., 2016) and e) Europa gridded ERSSTv4 (Liu et al., 2015). Anomalies were calculated relative to the 1981 to 2010 average bimonthly seasonal cycle for proxy reconstructions, instrumental SST and air temperatures.

Biogeosciences Discuss., https://doi.org/10.5194/bg-2018-441
Manuscript under review for journal Biogeosciences
Discussion started: 16 October 2018

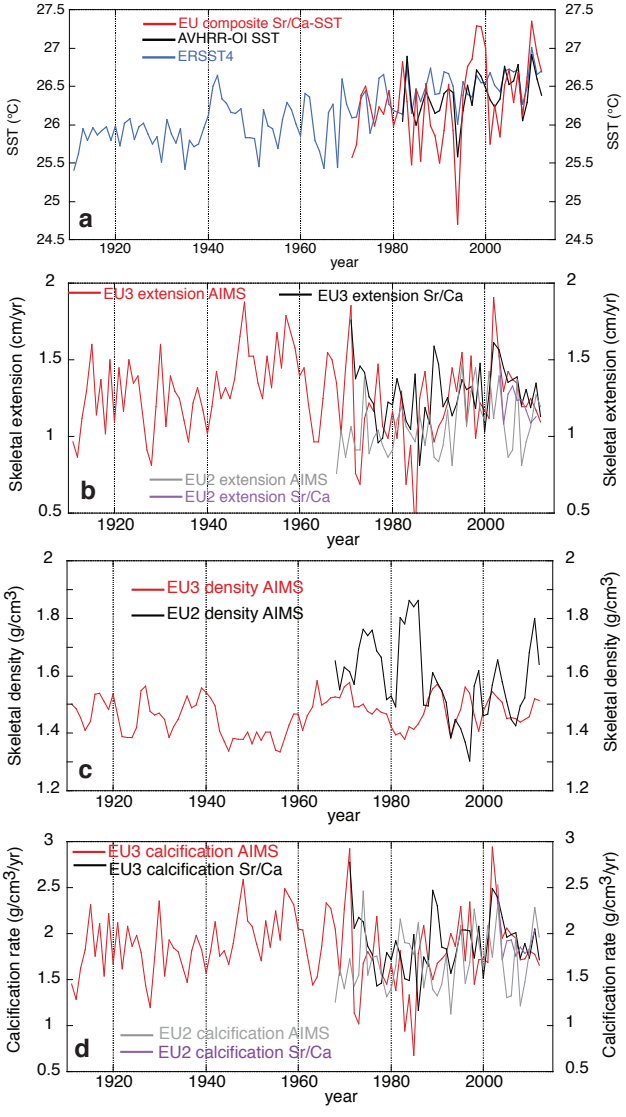

Figure 8 - Mean annual coral growth parameters of cores EU3 and EU2 compared to coral composite Sr/Ca-SST reconstruction, AVHRR-OISSTv2 (Banzon et al., 2016) and ERSSTv4 (Liu et al., 2015). a) mean annual SST time series, b) linear extension rate, c) skeletal density and d) calcification rate.

Biogeosciences Discuss., https://doi.org/10.5194/bg-2018-441
Manuscript under review for journal Biogeosciences
Discussion started: 16 October 2018

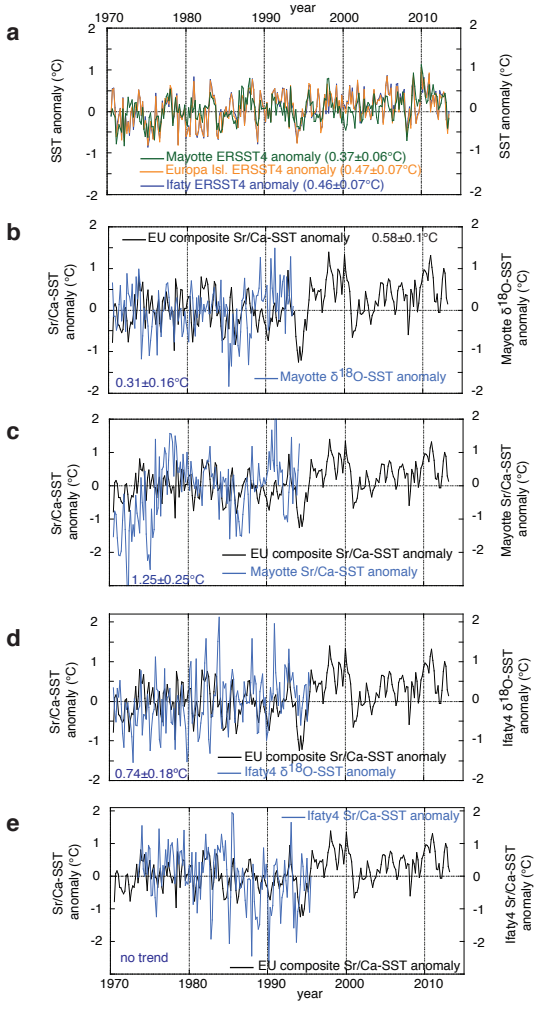

Figure 9 - Regional comparison of Mozambique Channel ERSSTv4 anomalies for Mayotte (green), Europa (orange) and Ifaty Reef, Madagascar (blue) in a) with linear warming trends in brackets. EU Sr/Ca-SST composite anomaly compared with b) Mayotte δ^{18}O-SST anomaly (blue), c) Mayotte Sr/Ca-SST anomaly (blue), d) Ifaty δ^{18}O -SST anomaly (blue) and e) Ifaty Sr/Ca-SST anomaly (blue). Anomalies were calculated for the 1973 to 1993 reference period. Linear warming trends indicated in b) to e) for proxy-SST for individual record length with EU composite Sr/Ca-SST anomaly only indicated once in panel b. Proxy data taken from Zinke et al. (2004, 2008).

Biogeosciences Discuss., https://doi.org/10.5194/bg-2018-441
Manuscript under review for journal Biogeosciences
Discussion started: 16 October 2018

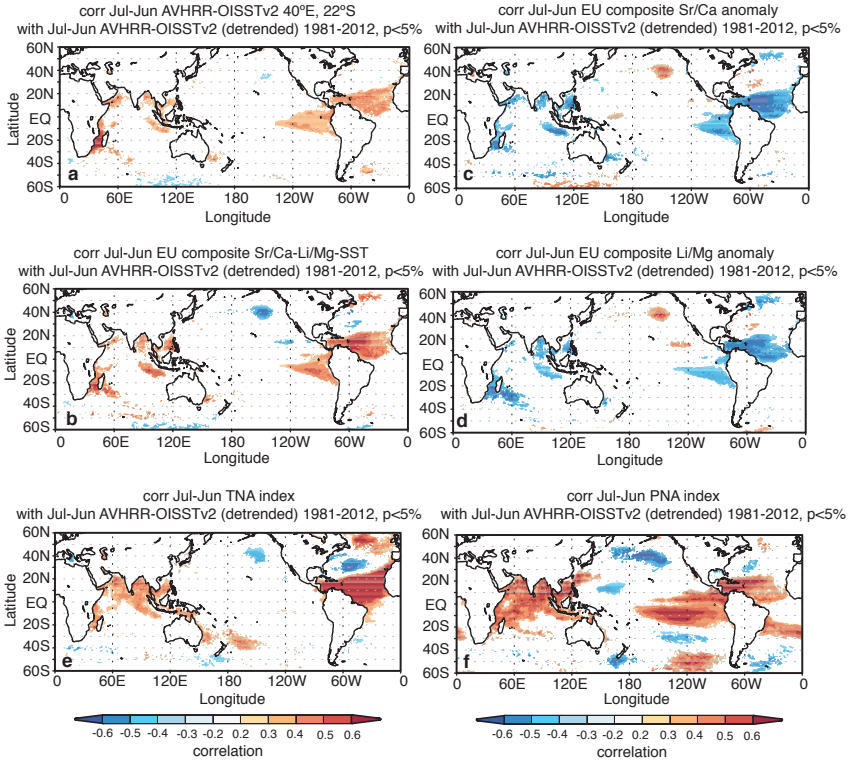

Figure 10 - Spatial correlations of proxy-based coral composite SST reconstructions with local and global AVHRR-OISSTv2 for mean annual data (Banzon et al., 2016). a) local AVHRR-OISSTv2 with global AVHRR-OISSTv2, b) local AVHRR-OISSTv2 with EU composite Sr/Ca-Li/Mg-SST, c) local AVHRR-OISSTv2 with EU composite Sr/Ca ratios and d) local AVHRR-OISSTv2 with EU composite Li/Mg ratios. Panels e and d show spatial correlations of the TNA and PNA indices with global AVHRR-OISSTv2. Only correlations with $p<0.05$ were coloured.

631